

Active Uncertainty Reduction for Safe and Efficient Interaction Planning: A Shielding-Aware Dual Control Approach

Journal Title
XX(X):1–24
©The Author(s) 2022
Reprints and permission:
sagepub.co.uk/journalsPermissions.nav
DOI: 10.1177/ToBeAssigned
www.sagepub.com/

SAGE

Haimin Hu¹, David Isele², Sangjae Bae², and Jaime F. Fisac¹

Abstract

The ability to accurately predict the opponent's behavior is central to the safety and efficiency of robotic systems in interactive settings, such as human-robot interaction and multi-robot teaming tasks. Unfortunately, robots often lack access to key information on which these predictions may hinge, such as opponent's goals, attention, and willingness to cooperate. Dual control theory addresses this challenge by treating unknown parameters of a predictive model as stochastic hidden states and inferring their values at runtime using information gathered during system operation. While able to optimally and automatically trade off exploration and exploitation, dual control is computationally intractable for general interactive motion planning, mainly due to the fundamental coupling between robot trajectory optimization and inference of opponent's intent. In this paper, we present a novel algorithmic approach to enable active uncertainty reduction for interactive motion planning based on the implicit dual control paradigm. Our approach relies on sampling-based approximation of stochastic dynamic programming, leading to a model predictive control problem that can be readily solved by real-time gradient-based optimization methods. The resulting policy is shown to preserve the dual control effect for a broad class of predictive models with both continuous and categorical uncertainty. To ensure the safe operation of the interacting agents, we leverage a supervisory control scheme, oftentimes referred to as "shielding", which overrides the ego agent's dual control policy with a safety fallback strategy when a safety-critical event is imminent. We then augment the dual control framework with an improved variant of the recently proposed shielding-aware robust planning scheme, which proactively balances the nominal planning performance with the risk of high-cost emergency maneuvers triggered by low-probability opponent's behaviors. We demonstrate the efficacy of our approach with both simulated driving examples and hardware experiments using 1/10 scale autonomous vehicles.

Keywords

Planning under uncertainty, human-robot interaction, dual control theory, stochastic MPC, safe learning.

1 Introduction

Computing robot plans that account for possible interactions with one or multiple opponents is a challenging task, as the robotic system and the opponent agents may have coupled dynamics, limited communication capabilities, and conflicting interests. Examples of interaction planning under uncertainty include human-robot interaction [Fisac et al. \(2018a\)](#); [Sadigh et al. \(2018\)](#); [Bajcsy et al. \(2021\)](#), multi-robot teaming [Leonard et al. \(2007\)](#); [Tokekar et al. \(2016\)](#); [Santos et al. \(2018\)](#), swarm robotics [Swain et al. \(2011\)](#); [Rubenstein et al. \(2014\)](#); [Chung et al. \(2018\)](#), autonomous racing [Liniger et al. \(2015\)](#); [Kabzan et al. \(2019\)](#); [Schwartz et al. \(2021\)](#), and mixed-autonomy traffic [Isele \(2019\)](#); [Bae et al. \(2020\)](#); [Wu et al. \(2021\)](#). To achieve safety and efficiency in those scenarios, the robot must competently predict and seamlessly adapt to the opponent's behavior. Intent-driven behavior models are widely used for such predictions: for example, the Boltzmann model [Luce \(1959\)](#); [Ziebart et al. \(2008\)](#) is commonly used for motion prediction of noisily rational decision makers. This model assumes that the opponent agent is exponentially more likely to take actions with a higher underlying *utility*. If the opponent's intent is well captured by a given utility function, the interaction can be modeled as a dynamic game in which the players' feedback

strategies can be obtained via dynamic programming [Fisac et al. \(2019\)](#). However, typical interaction settings may admit a plethora of *a priori* plausible intents (e.g., corresponding to distinct equilibrium solutions [Peters et al. \(2020\)](#) or different opponent's preferences [Sadigh et al. \(2018\)](#)), which in general cannot be fully modeled, let alone observed, by the robot [Fisac et al. \(2018b\)](#). The robot may seek to represent the other agent's intent through a parametric model and then infer the value of these parameters as hidden states under a Bayesian framework [Fisac et al. \(2018b\)](#); [Tian et al. \(2022\)](#); [Hu et al. \(2022\)](#), but doing so tractably while planning through interactions is an open problem.

Multi-stage trajectory optimization with closed-loop Bayesian inference can be generally cast as a stochastic optimal control problem. An important aspect of stochastic control with hidden states is whether the computed policy generates the so-called *dual control* effect [Feldbaum \(1960\)](#);

¹Department of Electrical and Computer Engineering, Princeton, Princeton University, NJ 08544, USA

²Honda Research Institute, San Jose, CA 95134, USA

Corresponding author:

Haimin Hu, Department of Electrical and Computer Engineering, Princeton University, Princeton, NJ 08544, USA
Email: haiminh@princeton.edu

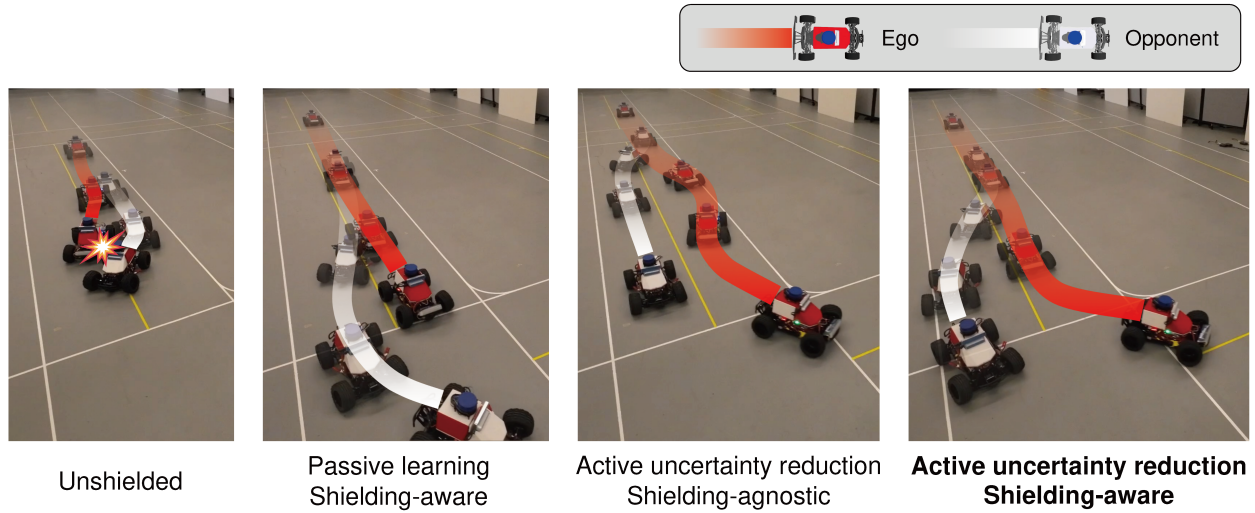


Figure 1. Safety and uncertainty reduction are two central components of interaction planning tasks, such as autonomous driving. Here, the ego autonomous car (red-front) seeks to overtake an opponent (white-front) autonomous car, whose control policy is unknown to the ego. The opponent car in this case is programmed as a cooperative agent, who will make way for the ego if they are sufficiently close. Four trials were controlled with roughly the same initial separation distance between the ego and the opponent. *Left:* An unshielded planner without formal safety guarantees is not able to guarantee collision-free maneuvers. *Middle-left:* A shielding-aware planner reasons about future shielding events and avoids relying on safety override if possible. However, a lack of active uncertainty reduction can cause the ego agent to be overly conservative and fail to complete the overtaking task. *Middle-right:* A shielding-agnostic policy with active uncertainty reduction produces aggressive overtaking maneuvers and triggers “near-miss” emergency overrides at the cost of performance and comfort. *Right:* Our proposed control framework combines active uncertainty reduction and shielding-aware planning, which balances safety and efficiency, leading to significant performance improvement for the closed-loop system.

Bar-Shalom and Tse (1974); Mesbah (2018); that is, in the context of interaction planning, whether the robot *actively* seeks to reduce the uncertainty about opponent’s hidden states. Solution methods for dual stochastic optimal control problems can be categorized into *explicit* approaches Heirung et al. (2015); Sadigh et al. (2018); Tian et al. (2021), which reformulate the problem with some form of heuristic probing, and *implicit* approaches Bar-Shalom and Tse (1974); Klenske and Hennig (2016); Arcari et al. (2020a), which directly tackle the control problem with stochastic dynamic programming. While explicit dual control problems are in general easier to formulate and solve than their implicit counterparts, designing the probing term and tuning its weighting factor can be non-trivial and may lead to inconsistent performance. For a comprehensive review of dual control methods, we refer to Mesbah (2018).

Contribution: In this paper, we formulate a broad class of interactive planning problems in the framework of stochastic optimal control and present an approximate solution method using implicit dual stochastic model predictive control (SMPC). The resulting policy automatically trades off the cost of exploration and exploitation, allowing the robot to actively reduce the uncertainty about the opponent’s hidden states without sacrificing expected planning performance. Our proposed SMPC problem supports both continuous and categorical opponent uncertainty and can be solved using off-the-shelf real-time nonlinear optimization solvers. To the best of our knowledge, this is the first interactive motion planning framework that performs active uncertainty reduction without requiring an explicit information-gathering strategy or objective.

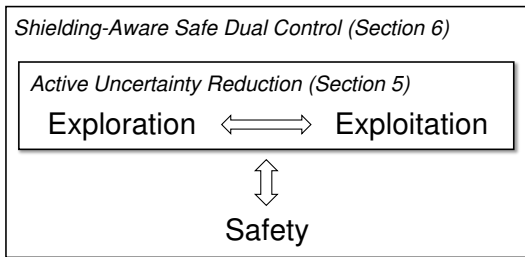
In order to provide formal safety guarantees for the ego robotic system and its opponents, we use the dual control

policy in conjunction with shielding, a supervisory safety filter scheme that overrides the dual controller with a safe backup policy. We improve the recently proposed shielding-aware robust planning (SHARP) framework from Hu et al. (2022), which generates efficient motions by reasoning about future shielding events triggered by low-probability opponent’s actions, to explicitly account for the opponent’s responses to the ego agent’s probing actions. We propose an easy-to-optimize convex constraint that locally captures the system evolution governed by high-cost safety maneuvers, and integrates it into the implicit dual SMPC formulation. The central ideas of our method are demonstrated in Fig. 1. *Our key insight is that the shielding-aware dual control policy simultaneously gathers useful information by actively engaging with the opponent, while remaining vigilant about the risk of efficiency loss due to costly shielding overrides.*

A preliminary version of this work Hu and Fisac (2022) was presented at the *International Workshop on the Algorithmic Foundations of Robotics (WAFR)*, 2022. In this revised and extended paper, we provide the following additional contributions: (i) an extension to general interaction planning problems (a superclass of the human-robot interaction planning problem considered in the original paper), (ii) more in-depth explanation, derivation, and analysis of the proposed framework, including more detailed discussions on the choice of opponent’s behavior models and properties of the proposed policy, (iii) incorporation of the shielding-aware robust planning scheme, which provides robust safety guarantees and reconciles conflicts between safety overrides and dual control probing actions, (iv) additional simulation results using the Waymo Open Motion Dataset Sun et al. (2020), and (v) hardware demonstration on 1/10 scale autonomous vehicles.

Table 1. Comparison of selected interaction planning methods that explicitly model coupled motions between agents.

Features	Schildbach and Borrelli (2015)	Sadigh et al. (2018)	Peters et al. (2020)	Tian et al. (2021)	Sunberg and Kochenderfer (2022)	Ours
Active uncertainty reduction	N	Y	N	Y	Y	Y
Automatic exploration-exploitation trade-off	N/A	N	N/A	Y	Y	Y
Safety guarantees	Y	N	N	N	N	Y
Continuous state space	Y	Y	Y	N	Y	Y
Continuous action space	Y	Y	Y	N	N	Y
Can handle more than one opponent	Y	N	Y	N	Y	Y
Can compute policy fully online	Y	Y	Y	N	Y	Y
Game-theoretic	N	Y	Y	Y	N	Y

**Figure 2.** Elements of interaction planning tasks and their relationships studied in the paper. In Section 5, we focus on dual control–based active uncertainty reduction that improves planning efficiency by balancing exploration and exploitation. In Section 6, we introduce shielding-aware safe dual control, which reconciles potential conflicts between safety and efficiency.

2 Related Work

In this section, we provide a literature review on different aspects of interaction planning methods. In Table 1, we compare planning strategies that explicitly account for the interaction between the ego and opponent agents. A diagram summarizing our algorithmic approach is shown in Fig. 2.

2.1 Interaction Planning as a POMDP

Robotic motion planning problems that involve identification of opponents’ behaviors governed by their unknown intentions can be modeled as a Mixed Observability Markov Decision Process Bandyopadhyay et al. (2013), a variant of the well-known Partially Observable Markov Decision Process (POMDP) Ong et al. (2009). Although intractable in the general form, efficient algorithms such as POMCP Silver and Veness (2010), DESPOT Ye et al. (2017), and POMCPOW Sunberg and Kochenderfer (2018) have been developed to approximately solve POMDPs. An approximate POMDP solution method based on POMCPOW is developed in Sunberg and Kochenderfer (2022) for safe, efficient, and highly scalable autonomous freeway driving. In Sehr and Bitmead (2017), a dual SMPC method is proposed to solve moderate-sized POMDPs. The resulting policy naturally exhibits system probing and automatically trades off exploration and exploitation. When interactions between the robot and the human are modeled, the POMDP formulation becomes a (usually intractable) Partially-Observable Stochastic Game (POSG) Sadigh et al. (2018). Our approach can be viewed as a new

computationally efficient framework for solving interaction planning problems cast as POSGs.

2.2 Human-in-the-Loop Motion Planning

Human-robot interaction, or human-in-the-loop planning, is an emerging and rapidly growing subfield of interaction planning. Traditional human-robot interaction planning algorithms usually adopt a two-stage pipeline, where human’s future motion is first reasoned with a predictive model, which is then fed into a motion planner. In Fisac et al. (2018b), the human’s future trajectories are predicted using the Boltzmann rationality model, and model confidence is concurrently estimated using Bayesian inference. This information is then used by a motion planner to obtain probabilistic collision-free guarantees. This framework is then extended in Tian et al. (2022) to explicitly account for game-theoretic models, in which the human’s role is also inferred, leading to a less conservative planning performance. Despite being computationally efficient, the above two-stage pipeline decouples inference from planning, which may lead to conservativeness in planning. Recently, efforts have been made towards a more integrated framework by solving a joint prediction-planning problem. In Sadigh et al. (2018), the authors propose to model human-robot interaction as a dynamical system, in which the robot’s action can affect the human’s action, thus producing predictions of the human’s future states. Related work in the following years proposes to solve the joint problem as a general-sum dynamic game Fisac et al. (2019); Fridovich-Keil et al. (2020); Zanardi et al. (2021). Our method falls into the category of joint prediction and planning.

2.3 Dual Stochastic Model Predictive Control

SMPC has been widely used for robotic motion planning under uncertainty due to its ability to handle safety-critical constraints and general uncertainty models. Seminal work Bernardini and Bemporad (2011) establishes a general framework for solving SMPC problems with scenario optimization. In Schildbach and Borrelli (2015), an SMPC approach is proposed for lane change assistance of the ego vehicle in the presence of other human-driven vehicles, whose future movements are predicted and incorporated as finitely many scenarios in the MPC formulation. SMPC is also used for autonomous driving at traffic intersections Nair et al. (2021), where the trajectories of other vehicles are predicted with Gaussian Mixture Models. In Chen et al.

(2022), a scenario-based SMPC algorithm is proposed to capture multimodal reactive behaviors of uncontrolled human agents. In [Hu et al. \(2022\)](#), a provably safe SMPC planner is developed for robust human-aware robotic motion planning, which proactively balances expected performance with the risk of high-cost emergency safety maneuvers triggered by low-probability human behaviors. However, all those SMPC methods do not produce dual control effect - the robot only passively adapts to predicted opponent's motion but will not actively probe the other agents to gather more information and reduce their uncertainty. In [Arcari et al. \(2020a\)](#), an implicit dual SMPC is proposed for optimal control of nonlinear dynamical systems with both parametric and structural uncertainty. In [Bonzanini et al. \(2020\)](#), a robust scenario-based SMPC is formulated to enable safe learning of a nonlinear dynamical system, whose dynamics are partially unknown and learned from data based on a Gaussian Process model. A novel state- and input-dependent scenario tree is used to account for the dependency of the uncertainty model on decision variables, which leads to active uncertainty reduction and improved closed-loop performance. Our paper builds on those dual SMPC approaches to enable active uncertainty reduction for interaction planning.

2.4 Active Information Gathering

To date, most interaction planning methods follow a “passively adaptive” paradigm. In [Peters et al. \(2020\)](#), a multi-agent interaction planning problem is modeled as a general-sum differential game with equilibrium uncertainty. The robot first infers which equilibrium the opponents are operating at and then aligns its own strategy with the inferred opponent's equilibrium solution. Recently, the notion of active information gathering, which is conceptually very similar to dual control, has received attention from the robotics, and in particular the human-robot interaction community. In [Sadigh et al. \(2018\)](#), an additional information gathering term is added to the robot's nominal objective in a trajectory optimization framework for online estimating unknown parameters of the human's state-action value function. In fact, according to the categorization proposed by [Mesbah \(2018\)](#), the method in [Sadigh et al. \(2018\)](#) can be classified as an explicit dual control approach, which requires heuristic design of a probing mechanism and weighing the relative importance between optimizing the expected performance and reducing the uncertainty of human's unknown parameters. On the contrary, we propose an implicit dual control approach, which automatically balances performance with uncertainty reduction, thus not requiring design of a heuristic information gathering mechanism.

2.5 Safe Interaction Planning via Shielding

One popular way of improving safety for motion planning under uncertainty is through chance constraint or probabilistically safe planning [Schildbach and Borrelli \(2015\)](#); [Fisac et al. \(2018b\)](#); [Bastani et al. \(2021\)](#). However, using a probabilistically safe planning policy, safety can still be breached when the opponent takes low-probability actions. This is also known as the issue of the “long tail” of

unlikely events [Koopman \(2018\)](#). All-time safety in interaction planning can be guaranteed by a least-restrictive supervisory control scheme, often referred to as *shielding*. In this paradigm, a reactive safety fallback policy is used as the “last resort”, which overrides the nominal policy *only when* a safety-critical event, e.g. a collision, is imminent. Commonly used shielding mechanisms include, for example, Hamilton-Jacobi (HJ) Reachability analysis [Mitchell et al. \(2005\)](#); [Bansal et al. \(2017\)](#), control barrier functions [Ames et al. \(2016\)](#); [Robey et al. \(2020\)](#), model predictive control [Li and Bastani \(2020\)](#); [Wabersich and Zeilinger \(2021\)](#), and Lyapunov methods [Chow et al. \(2018\)](#). Despite being effective at guaranteeing safety, shielding can sometimes degrade the planning efficiency, since the safety controllers are typically designed without performance considerations such as task completion time, smoothness of the trajectory or power consumption. To mitigate this issue, the shielding-aware robust planning (SHARP) framework is developed in [Hu et al. \(2022\)](#), which proactively balances the nominal planning performance with costly emergency maneuvers triggered by low-probability opponent's behaviors. In this paper, we incorporate SHARP into implicit dual SMPC for safe and efficient interaction planning, and improve it by lifting the overly conservative assumption that the opponent ignores the ego agent, and explicitly accounting for opponent's responses to the ego agent's probing action.

3 Preliminaries

3.1 Multi-Agent Dynamical System

We consider a class of discrete-time input-affine dynamics that capture the interaction between an ego robotic system (e) and an individual *or a group of* opponent agent (o), e.g. human or other robots,

$$x_{t+1} = f(x_t) + B^e(x_t)u_t^e + B^o(x_t)u_t^o + d_t, \quad (1)$$

where $x_t = (x_t^e, x_t^o) \in \mathbb{R}^n$ is the joint state vector, $u_t^e \in \mathcal{U}^e \subseteq \mathbb{R}^{m_e}$ and $u_t^o \in \mathcal{U}^o \subseteq \mathbb{R}^{m_o}$ are the control vectors of the ego and the opponent, respectively, $f: \mathbb{R}^n \rightarrow \mathbb{R}^n$ is a nonlinear function that describes the autonomous part of the dynamics, $B^e: \mathbb{R}^n \rightarrow \mathbb{R}^{n \times m_e}$ and $B^o: \mathbb{R}^n \rightarrow \mathbb{R}^{n \times m_o}$ are control input matrices that can depend on the state, and d_t is an additive uncertainty term representing external disturbance inputs (e.g. wind) and modeling error. For simplicity, we further assume that $d_t \sim \mathcal{N}(0, \Sigma^d)$ is a zero-mean i.i.d. Gaussian random variable.

Remark 1. Dynamics (1) model multiple opponent systems o_1, o_2, \dots by concatenating their state and control vectors, i.e. $x^o = (x^{o_1}, x^{o_2}, \dots)$ and $u^o = (u^{o_1}, u^{o_2}, \dots)$.

3.2 Modeling Opponent Behaviour

In this paper, we parametrize the opponent's action at each time t as a stochastic policy:

$$u_t^o := \sum_{i=1}^{n_\theta} \theta_i^M u_i^{M,o}, \quad \text{subject to } u_t^o \in \mathcal{U}^o, \quad (2)$$

which is a linear combination of *stochastic basis policies* $u_i^{M,o}$ with parameter $\theta^M := (\theta_1^M, \theta_2^M, \dots, \theta_{n_\theta}^M) \in \mathbb{R}^{n_\theta}$. We further allow each basis policy $u_i^{M,o}$ to have different *modes* M that take values from a *finite* set \mathcal{M} , representing

different categorical behaviors of the opponent (such as being cooperative, non-cooperative, or unaware). We define each basis policy $u_i^{M,o}$ with the “noisily-rational” Boltzmann model from cognitive science [Luce \(1959\)](#). Under this model, the opponent picks each basis policy according to a probability distribution:

$$u_i^{M,o} \sim p(u_i^{M,o} | x, u^e; M) = \frac{e^{-Q_i^M(u_i^{M,o}; x, u^e)}}{\int_{\tilde{u}^o \in \mathcal{U}^o} e^{-Q_i^M(\tilde{u}^o; x, u^e)} d\tilde{u}^o},$$

for all $i = 1, 2, \dots, n_\theta$ and $M \in \mathcal{M}$. Here, $Q_i^M(u_i^{M,o}; x, u^e)$ is the opponent’s basis state-action value (or Q-value) function associated with the i -th basis policy and mode M . This model assumes that, for a pair of fixed (i, M) , the opponent is exponentially likelier to pick an action that maximizes the state-action value function.

Remark 2. Rational decision makers (e.g. robots) are a special case of noisily-rational agents when they choose actions according to $u_i^{M,o} = \arg \max Q_i^M(\cdot)$, i.e. there is no uncertainty (ambiguity) when picking basis policies $u_i^{M,o}$, while the uncertainties in model parameters (θ^M, M) and external disturbance inputs d still persist. Therefore, our framework can naturally account for rational opponents.

Remark 3. Our approach is agnostic to the concrete methods for determining the opponent’s state-action value function $Q_i^M(\cdot)$, parameters θ^M and M , which are usually specified by the system designer based on domain knowledge or learned from prior data. Goal-driven models of opponent motion are well-established in the literature. See for example [Sadigh et al. \(2018\)](#); [Ziebart et al. \(2008\)](#). We provide two examples below.

Example 1. (Robot opponent with an unknown policy). Consider on an RC car test track (Figure 1 and 14) the ego car is tasked to overtake an opponent robot car controlled by an MPC policy unknown to the ego. Following Section 3.2, we parametrize the opponent’s state-action value function as

$$u_t^o = \theta_{tr}^M u_{tr}^M(x_t, u_t^e) + \theta_{sa}^M u_{sa}^M(x_t, u_t^e), \quad \text{s.t. } u_t^o \in \mathcal{U}^o,$$

where $\theta^M := (\theta_{tr}^M, \theta_{sa}^M)$, basis policies $u_{tr}^M(\cdot)$ and $u_{sa}^M(\cdot)$ capture the opponent’s tracking (e.g. following the reference trajectory) and safety (e.g. avoiding collision with the ego) objectives, respectively. Modeling the opponent’s level of commitment to safety as a continuum is motivated by recent work [Toghi et al. \(2021, 2022\)](#). Further, the opponent has two distinct modes, namely willing to yield to the ego by changing the lane or not, i.e. $M \in \{Y, NY\}$. An illustration of opponent’s behaviors modeled by different modes and configurations of basis policies can be found in Fig. 3.

Example 2. (Game-theoretic human-robot interaction). In the second example, we consider a traffic intersection scenario that involves an autonomous vehicle (ego) and a pedestrian (opponent). We model the pedestrian as a game-theoretic decision maker using model (2) with parameter $\theta^M := (\theta_C^M, \theta_{NC}^M)$, which captures the opponent’s level of cooperativeness. A cooperative opponent also optimizes for the robot’s objective while a non-cooperative opponent does not. We define the discrete modes M as different (game-theoretic) interactive behaviors of the opponent toward

the robot, similar to [Bandyopadhyay et al. \(2013\)](#); [Tian et al. \(2022\)](#). Specifically, the opponent’s state-action value function is defined as

$$Q_i^M = \begin{cases} Q_i^M(u_i^{M,o}; x_t, u_t^{e, \text{Nash}}(x_t)), & \text{if } M = N, \\ Q_i^M(u_i^{M,o}; x_t, u_t^{e, \text{worst}}(x_t)), & \text{if } M = p, \\ Q_i^M(u_i^{M,o}; x_t, u_t^{e, \text{best}}(x_t)), & \text{if } M = w, \\ Q_i^M(u_i^{M,o}; x_t^o), & \text{if } M = o. \end{cases}$$

In the first three modes, the opponent assumes that the robot’s control u_t^e is a (local) feedback Nash equilibrium solution [Başar and Olsder \(1998\)](#) ($M = N$), the worst-case one that minimizes $Q_i^M(\cdot)$ (i.e. a protected opponent with $M = p$), and the best-case one that maximizes $Q_i^M(\cdot)$ (i.e. a wishful opponent with $M = w$), respectively; the last mode follows the same assumption as in [Fisac et al. \(2018b\)](#); [Bajcsy et al. \(2021\)](#); [Hu et al. \(2022\)](#) that the opponent is oblivious and ignores the presence of other agents ($M = o$).

3.3 Inferring Model Parameter

In general, parameter θ^M and mode M in opponent action model (2) are *hidden states* that are unknown to the robot. Therefore, they can only be inferred from past observations. To address this, we define the information vector $\mathcal{I}_t := [x_t, u_{t-1}^e, \mathcal{I}_{t-1}]$ as the collection of all information that is *causally observable* by the robot at time $t \geq 0$, with $\mathcal{I}_0 = [x_0]$. We then define the *belief state* $b_t := p(\theta^M, M | \mathcal{I}_t)$ as the joint distribution of (θ^M, M) conditioned on \mathcal{I}_t , and $b_0 := p(\theta^M, M)$ is a given prior distribution. When the ego agent receives a new observation $x_{t+1} \in \mathcal{I}_{t+1}$, the current belief state b_t is updated using the recursive Bayesian inference equations:

$$\begin{aligned} p(\theta_{-}^M | \mathcal{I}_{t+1}; M) &= \frac{p(x_{t+1} | u_t^e, \mathcal{I}_t; \theta_{-}^M, M) p(\theta_{-}^M | \mathcal{I}_t; M)}{p(x_{t+1} | u_t^e, \mathcal{I}_t; M)}, \end{aligned} \quad (3a)$$

$$p(M_{-} | \mathcal{I}_{t+1}) = \frac{p(x_{t+1} | u_t^e, \mathcal{I}_t; M) p(M | \mathcal{I}_t)}{p(x_{t+1} | u_t^e, \mathcal{I}_t)}, \quad (3b)$$

$$b_{t+1}^{-} := p(\theta_{-}^M | \mathcal{I}_{t+1}; M) p(M_{-} | \mathcal{I}_{t+1}), \quad (3c)$$

$$b_{t+1} = g^t(b_{t+1}^{-}) := \int p(\theta^M, M | \tilde{\theta}_{-}^M, \tilde{M}_{-}) \cdot p(\tilde{\theta}_{-}^M, \tilde{M}_{-} | \mathcal{I}_{t+1}) d\tilde{\theta}_{-}^M d\tilde{M}_{-}. \quad (3d)$$

where b_{t+1}^{-} is the belief state updated with the likelihood $p(x_{t+1} | u_t^e, \mathcal{I}_t; M)$, $p(\theta^M, M | \tilde{\theta}_{-}^M, \tilde{M}_{-})$ is a transition model and $g^t(\cdot)$ is the belief state transition dynamics. We can compactly rewrite (3a)-(3d) as a dynamical system,

$$b_{t+1} = g(b_t, x_{t+1}, u_t^e). \quad (4)$$

Unfortunately, system (4) in general does not adopt an analytical form beyond one-step evolution. Even if the prior distribution b_t is a Gaussian, the posterior b_{t+1} ceases to be a Gaussian since the opponent’s action u_t^o defined by (2) (which in turn affects the observation x_{t+1}) is generally non-Gaussian, thus precluding the use of the conjugate-prior properties of Gaussian distributions. In Section 5, we will introduce a computationally efficient method to propagate the belief state dynamics approximately.

4 Problem Statement

4.1 Canonical Interaction Planning Problem

We now define the central problem we want to solve in this paper: the canonical interaction planning problem, which is formulated as a stochastic finite-horizon optimal control problem as follows:

$$\begin{aligned} \min_{\Pi^e} \quad & \mathbb{E}_{(\theta^M, M) \sim b_{[0:N-1]}, u_{[0:N-1]}^o \sim (2), d_{[0:N-1]}} \sum_{k=0}^{N-1} \ell(x_k, \pi_k^e(x_k, b_k)) + \ell_F(x_N) \\ \text{s.t.} \quad & x_0 = \hat{x}_t, b_0 = \hat{b}_t, \\ & \forall k = 0, \dots, N-1: \\ & x_{k+1} = f(x_k) + B^e \pi_k^e + B^o u_k^o + d_k, \\ & b_{k+1} = g(b_k, x_{k+1}, \pi_k^e(x_k, b_k)), \\ & x_k \notin \mathcal{F}, \quad \forall k = 0, \dots, N \end{aligned} \quad (5a) \quad (5b) \quad (5c) \quad (5d) \quad (5e)$$

where $\Pi^e = \{\pi_0^e(\cdot), \dots, \pi_{N-1}^e(\cdot)\}$ is the policy sequence obtained by optimizing (5), \hat{x}_t and \hat{b}_t are the state measured and belief state maintained at *real-world time* t , the *prediction time* associated with decision variables is indexed with k , $\ell: \mathbb{R}^n \times \mathcal{U}^e \rightarrow \mathbb{R}_{\geq 0}$ and $\ell_F: \mathbb{R}^n \rightarrow \mathbb{R}_{\geq 0}$ are designer-specified stage and terminal cost function, $\pi_k(x_k, b_k)$ is a *causal* feedback policy Bar-Shalom and Tse (1974); Mesbah (2018) that leverages the (yet-to-be-acquired) knowledge of future states $x_{[k, \dots, N]}$ and belief states $b_{[k, \dots, N-1]}$, and $\mathcal{F} \subseteq \mathbb{R}^n$ is a failure set that the state is not allowed to enter.

For the moment, we drop the safety constraint (5e) and defer the discussion of how to tractably enforce it to Section 6. Now, problem (5) can be solved using stochastic dynamic programming Bellman (1966). An optimal robot's value function (minimum cost-to-go) $V_k(x_k, b_k)$ and control policy $\pi_k^{e,*}(x_k, b_k)$ can be obtained backward in time using the Bellman recursion,

$$\begin{aligned} V_k(x_k, b_k) = \min_{\pi_k^e(x_k, b_k)} \ell(x_k, \pi_k^e) + \mathbb{E}_{(\theta^M, M) \sim b_k, u_k^o \sim (2), d_k} [V_{k+1}(x_{k+1}, b_{k+1}) | \mathcal{I}_k] \\ \text{s.t. (5c) - (5e)} \end{aligned} \quad (6)$$

with terminal condition $V_N(x_N, b_N) = \ell_F(x_N)$.

4.2 Dual Control Effect

Value function $V_t(x_t, b_t)$ obtained by solving (6) depends on future belief states $b_{t'}$ ($t' > t$), thus giving the optimal policy the ability to affect *future uncertainty* of the opponent quantified by the belief states. Therefore, the optimal policy $u_t^{e,*}$ of (6) possesses the property of *dual control effect*, defined formally in Definition 1. Due to the principle of optimality Bellman (1966), the policy achieves an optimal balance between optimizing the robot's expected performance objective (5a) and actively reducing its uncertainty about the opponent. In other words, the optimal policy of (6) automatically probes the opponent agents to reduce their associated uncertainty *only* to the extent that doing so improves the robot's expected closed-loop performance.

Definition 1. Dual Control Effect. A control input has dual control effect if it can affect, with nonzero probability,

- (a) At least one r th-order ($r \geq 2$) central moment of a hidden state variable Feldbaum (1960); Bar-Shalom and Tse (1974); Mesbah (2018), or
- (b) Entropy of a categorical hidden state variable Hijab (1984).

4.3 Approximate Dual Control

Unfortunately, (6) is computationally intractable in all but the simplest cases, mainly due to nested optimization of robot's action and computing the conditional expectation. The expectation term in (6) can be approximated to arbitrary accuracy with quantization of the belief states, which, however, leads to exponential growth in computation, i.e. the issue of *curse of dimensionality* Bellman (1966). It is for those reasons that approximate methods are mainly used to solve dual control problems. Approximate dual control can be categorized into: explicit approaches, e.g. Heirung et al. (2015); Sadigh et al. (2018); Tian et al. (2021) that simplify the original stochastic optimal control problem by artificially introducing probing effect or information gathering objectives to the control policy, and implicit approaches, e.g. Bar-Shalom and Tse (1974); Klenske and Hennig (2016); Arcari et al. (2020a) that rely on direct approximation of the Bellman recursion (6). The approach we take in this paper is a *scenario-based implicit dual control method*, which is detailed in the next section. The main advantage of using the implicit dual control approximation is that the automatic exploration-exploitation trade-off of the policy is naturally preserved in an optimal sense Sehr and Bitmead (2017); Mesbah (2018).

5 Active Uncertainty Reduction using Implicit Dual Control

In this section, we describe an implicit dual control approach towards approximately solving the canonical interaction planning problem (5). We start by presenting an approximation scheme for tractably propagating the belief state dynamics and computing the expectation in Bellman recursion (6). This is essential for reformulating (6) as a real-time solvable SMPC problem. The formulation of our proposed SMPC problem and properties of the resulting policy are detailed in Section 6.

5.1 Parameter-Affine Dynamics

In order to tractably propagate belief state dynamics (4), we propose to reformulate joint dynamics (1) into the *parameter-affine* form:

$$x_{t+1} = F(x_t, u_t^e) \theta^M + \bar{f}(x_t, u_t^e) + \bar{d}_t, \quad (7)$$

where the opponent control term $B^o(x_t)u_t^o$ in (1) is replaced with $F(x_t, u_t^e)\theta^M$, which is linear in parameter θ^M , and \bar{d}_t is a zero-mean Gaussian random variable, whose covariance can be different from the disturbance term d_t in (1). This serves as a key building block for deriving the approximate belief updating rule in Section 5.2.

To obtain parameter-affine dynamics, the main technical tool we rely on is the Laplace approximation (Bishop 2006, Chapter 4). Precisely, the conditional probability distribution of each opponent's basis policy $u_i^{M,o}$ is approximated as:

$$p(u_i^{M,o} | x_t, u_t^e; M) \approx \mathcal{N}(\mu_i^M(\cdot), \Sigma_i^M(\cdot)), \quad (8)$$

where the mean function of the basis policy is

$$\mu_i^M(x_t, u_t^e) := \arg \max_{u_i^{M,o} \in \mathcal{U}^o} Q_i^M(u_i^{M,o}; x_t, u_t^e),$$

and the covariance function of the basis policy is

$$\Sigma_i^M(x_t, u_t^e) := \nabla_{u_i^{M,o}}^2 Q_i^M(u_i^{M,o}; x_t, u_t^e) \Big|_{\mu_i^M(x_t, u_t^e)}^{-1}.$$

The intuition behind the above Laplace approximation scheme is that the Gaussian distribution obtained in (8) centers around the *mode* $\mu_i^M(x_t, u_t^e)$ of the original basis policy distribution $p(u_i^{M,o} | x_t, u_t^e; M)$, which corresponds to the *perfectly rational* opponent's action associated with θ_i^M . We discuss maximization of the basis Q-value function $Q_i^M(\cdot)$ in Appendix C.1. The overall *approximate* opponent's action distribution, conditioned on θ^M and M , is given by:

$$p(u_t^o | x_t, u_t^e; \theta^M) \approx \mathcal{N}(\mu_t^{u^o}(\cdot), \Sigma_t^{u^o}(\cdot)) \quad (9)$$

where the mean function of opponent's overall policy is

$$\mu_t^{u^o}(x_t, u_t^e; \theta^M) := \sum_{i=1}^{n_\theta} \theta_i^M \mu_i^M(x_t, u_t^e),$$

and the covariance function of opponent's overall policy is

$$\Sigma_t^{u^o}(x_t, u_t^e; \theta^M) := \sum_{i=1}^{n_\theta} (\theta_i^M)^2 \Sigma_i^M(x_t, u_t^e).$$

We subsequently lift the requirement that $u_t^o \in \mathcal{U}^o$ in order to keep u_t^o normally distributed *during belief propagation*, and we use a projected u_t^o for state evolution. We discuss how to deal with the unbounded support of predicted u_t^o in Appendix C.2. Based on the covariance function of u^o obtained above, we can compute the covariance of the disturbance term \bar{d}_t in parameter-affine dynamics (7) as

$$\Sigma_t^{\bar{d}}(x_t, u_t^e; \theta^M) := \Sigma^d + B^o \Sigma_t^{u^o}(x_t, u_t^e; \theta^M) B^{o\top}, \quad (10)$$

which captures the *combined* uncertainty stemmed from the external disturbance d_t in (1) and opponent's noisily-rational action u_t^o characterized by (9).

As the last step towards obtaining the parameter-affine dynamics, we define the *mean matrix* by concatenating the mean functions of opponent's basis policies:

$$U^o(x_t, u_t^e) := [\mu_1^M(x_t, u_t^e) \quad \dots \quad \mu_{n_\theta}^M(x_t, u_t^e)]. \quad (11)$$

Plugging (2) and (11) into (1) leads to:

$$x_{t+1} = \underbrace{B^o(x_t)U^o(x_t, u_t^e)\theta^M}_{=:F(x_t, u_t^e)} + \underbrace{f(x_t) + B^e(x_t)u_t^e}_{=:f(x_t, u_t^e)} + \bar{d}_t, \quad (12)$$

which is in form of parameter-affine dynamics (7).

Remark 4. Even if dynamics (12) are linear in parameter θ^M , dependence of covariance matrix $\Sigma_t^{\bar{d}}$ on θ^M , as shown in (10), still prohibits updating the belief states in closed-form. To this end, we approximate $\Sigma_t^{\bar{d}}$ by fixing θ^M with some estimated value $\bar{\theta}^M$. In our paper, we estimate $\bar{\theta}^M$ using a roll-out-based approach by setting its value to the mean of the conditional distribution of θ^M computed in Step 3 of the initialization pipeline described in Appendix C.3.

Remark 5. Alternative Opponent Action Model. In this paper, we mainly use model (2) (linear combination of basis policies) for predicting opponent's actions in simulation studies and experiments. Nonetheless, we highlight that our methodology applies to any opponent action model that can lead to parameter-affine dynamics (7). Here, we provide another action model that falls into such category. Similar to (Bobu et al. 2020, Section IV.A), consider the opponent's state-action value function* parametrized as a linear combination of basis functions:

$$Q_\theta^M(u^o; x, u^e, \theta^M) = \sum_{i=1}^{n_\theta} \theta_i^M Q_i^M(u^o; x, u^e),$$

and an associated noisily-rational Boltzmann model:

$$u_t^o \sim p(u^o | x, u^e; \theta^M) = \frac{e^{-Q_\theta^M(u^o; x, u^e, \theta^M)}}{\int_{\bar{u}^o \in \mathcal{U}^o} e^{-Q_\theta^M(\bar{u}^o; x, u^e, \theta^M)} d\bar{u}^o}.$$

We again leverage the Laplace approximation to locally approximate the above model as $p(u_t^o | x_t, u_t^e; \theta^M) \approx \mathcal{N}(\mu_t^{u^o}(x_t, u_t^e; \theta^M), \Sigma_t^{u^o}(x_t, u_t^e; \theta^M))$. We then perform a first-order Taylor expansion around a given $\bar{\theta}^M$:

$$\begin{aligned} \mu_t^{u^o}(\cdot) &\approx \nabla_{\theta^M} \mu_t^{u^o}(x, u^e; \theta^M) \Big|_{\bar{\theta}^M} \delta\theta^M + \bar{\mu}_t^{u^o}(x_t, u_t^e; \bar{\theta}^M) \\ &=: U^o(x, u^e) \delta\theta^M + \bar{\mu}_t^{u^o}(x_t, u_t^e; \bar{\theta}^M), \end{aligned}$$

where $\delta\theta^M := \theta^M - \bar{\theta}^M$ is the error term. This leads to parameter-affine dynamics in form of (7) with $F(x_t, u_t^e) = B^o(x_t)U^o(x_t, u_t^e)$ and $\bar{f}(x_t, u_t^e) = f(x_t) + B^e(x_t)u_t^e + B^o(x_t)\bar{\mu}_t^{u^o}(x_t, u_t^e; \bar{\theta}^M) - F(x_t, u_t^e)\bar{\theta}^M$.

5.2 Tractable Reformulation of Belief Updates

Given the parameter-affine dynamics in Section 5.1, we can now derive a tractable recursive update rule for the belief state dynamics (4). Since the support of θ^M is continuous, we model its conditional belief as a Gaussian, i.e. $p(\theta^M | \mathcal{I}_t; M) \sim \mathcal{N}(\mu_t^{\theta^M}, \Sigma_t^{\theta^M})$. Likewise, $p(M | \mathcal{I}_t)$ is modeled as a categorical distribution due to its discrete support \mathcal{M} .

Our central idea is to update $p(\theta^M | \cdot)$ efficiently leveraging the self-conjugate property (Bishop 2006, Appendix B) of Gaussian distributions, that is, given Gaussian prior $p(\theta^M | \mathcal{I}_t; M)$, if the likelihood $p(x_{t+1} | u_t^e, \mathcal{I}_t; \theta^M, M)$ is Gaussian, then the posterior $p(\theta_{t+1}^M | \mathcal{I}_{t+1}; M)$ is also Gaussian, whose mean and covariance are analytical functions of state x_t and ego's action u_t^e . The following lemma summarizes the approximate belief update procedure for $p(\theta^M | \cdot)$, whose proof can be found in Appendix B.1.

*In Bobu et al. (2020), the authors used a linear combination of basis cost (i.e. value) functions that only depend on the states instead of state-action value functions to model the opponent's behavior.

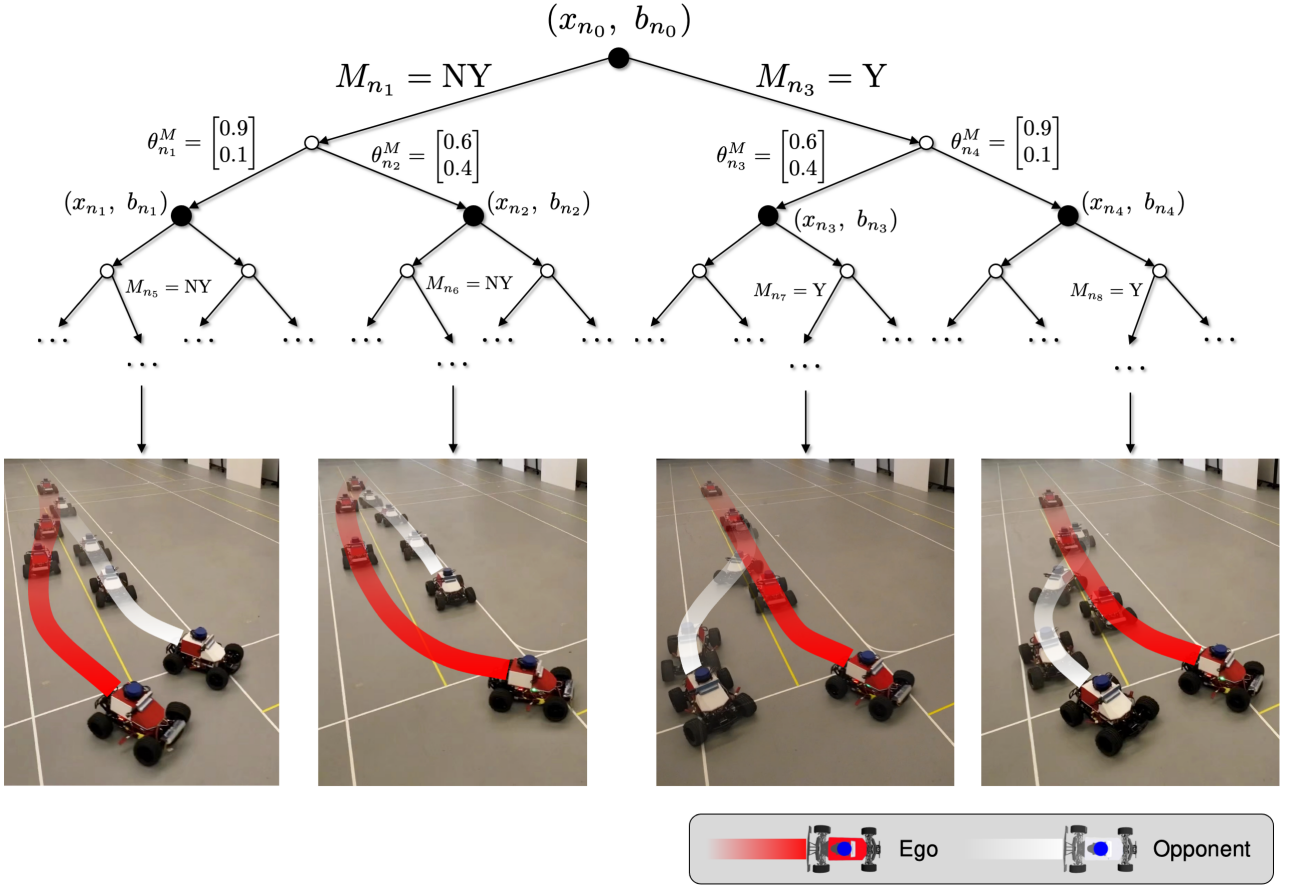


Figure 3. Illustration of an optimized scenario tree for Example 1. The ego and opponent vehicles are painted red front and white front, respectively. Uncertainty samples $M_{\tilde{n}}$ and $\theta_{\tilde{n}}^M$ associated with node \tilde{n} (see Section 5.3 for scenario tree notations) are used for approximately computing the stochastic objective (20a), and propagating belief states along each scenario branch. *Left scenario:* The opponent did not yield, and was less inclined to avoid colliding with the ego vehicle (sampled continuous hidden state $\theta_{tr}^M \gg \theta_{sa}^M$). *Middle-left scenario:* The opponent did not yield, but slowed down to avoid the ego vehicle. *Middle-right scenario:* The opponent yielded and made a wider turn to avoid hitting the ego vehicle. *Right scenario:* The opponent yielded, but was less inclined to avoid the ego vehicle.

Lemma 1. For the parameter-affine dynamics (7) and opponent's policy distribution $p(u_t^o | x_t, u_t^e; \theta^M)$ in (8), if the prior distribution of θ^M is given by $p(\theta^M | \mathcal{I}_t; M) \sim \mathcal{N}(\mu_t^{\theta^M}, \Sigma_t^{\theta^M})$, then the posterior distribution is $p(\theta^M | \mathcal{I}_{t+1}; M) \sim \mathcal{N}(\mu_{t+1}^{\theta^M}, \Sigma_{t+1}^{\theta^M})$ whose mean and covariance are given by

$$\begin{aligned} \mu_{t+1}^{\theta^M} &= \Sigma_{t+1}^{\theta^M} \left[F(x_t, u_t^e)^\top (\Sigma_{t+1}^x)^{-1} (x_{t+1} - \bar{f}(x_t, u_t^e)) \right. \\ &\quad \left. + (\Sigma_t^{\theta^M})^{-1} \mu_t^{\theta^M} \right] \\ \Sigma_{t+1}^{\theta^M} &= \left[(\Sigma_t^{\theta^M})^{-1} + F(x_t, u_t^e)^\top (\Sigma_{t+1}^x)^{-1} F(x_t, u_t^e) \right]^{-1} \end{aligned}$$

where $\Sigma_{t+1}^x := \Sigma^d + B^o(x_t) \Sigma_t^{u^o}(x_t, u_t^e; \theta^M) B^o(x_t)^\top$.

Importantly, the approximate belief state dynamics in Lemma 1 serve as an essential step towards preserving the dual control effect when approximately solving stochastic dynamic programming (6). This can be intuitively seen by inspecting that the robot's control u_t^e enters the updating equation of covariance matrix $\Sigma_{t+1}^{\theta^M}$. Therefore, u_t^e affects $\Sigma_{t+1}^{\theta^M}$ and all future covariance matrices implicitly by affecting future states $x_{t'}$ ($t' > t + 1$), hence producing dual control effect for θ^M according to Definition 1. A formal

proof of dual control effect provided by the SMPC policy using the approximate belief state dynamics in Lemma 1 can be found in Section 6 (Theorem 1). Measurement update (3b) for M can be readily computed by marginalizing the likelihood with respect to θ^M and subsequently applying the Bayes rule, similar to Arcari et al. (2020a). We denote the approximate belief state dynamics in compact form as

$$b_{t+1} = \tilde{g}(b_t, x_{t+1}, u_t^e), \quad (13)$$

which will later be used in SMPC as dynamics constraints for computationally tractable belief propagation.

5.3 Dynamic Scenario Trees

In this section, we propose an approximate solution method for the canonical interaction planning problem (5) using scenario tree-based stochastic model predictive control (ST-SMPC) Bernardini and Bemporad (2011), which yields a control policy with dual control effect. The key idea of ST-SMPC is to approximate the expectation in Bellman recursion (6) based on uncertainty samples, i.e. quantized belief states. This leads to a scenario tree that allows us to roll out (6) as a deterministic finite-horizon optimal control problem, which can be readily solved by gradient-based algorithms. Since our approach hinges on directly approximating Bellman recursion (6), it can be understood

Algorithm 1 Construct a scenario tree

Input: Current state \hat{x}_t and belief state \hat{b}_t , horizon $N > 0$, dual control horizon $1 \leq N^d \leq N$, mode set \mathcal{M} , branching number $K > 0$

Output: A scenario tree defined by node set \mathcal{N}_t

```

// Initialization:
1: Set  $x_{n_0} \leftarrow \hat{x}_t, b_{n_0} \leftarrow \hat{b}_t, t_{n_0} \leftarrow 0, \mathcal{N}_t \leftarrow \{n_0\}$ 
// Dual Control Steps:
2: for all  $t' = 0, 1, \dots, N^d$  do
3:   for all  $\tilde{n} \leftarrow \mathcal{N}_t$  do
4:     if  $\tilde{n}.t = t'$  then
5:       Branching:  $\mathcal{N}_t \leftarrow \mathcal{N}_t \cup \text{BRANCH}(\tilde{n}, \mathcal{M}, K)$ 
6:     end if
7:   end for
8: end for
// Exploitation Steps:
9: for all  $t' = N^d, N^d + 1, \dots, N$  do
10:  for all  $\tilde{n} \leftarrow \mathcal{N}_t$  do
11:    if  $\tilde{n}.t = t'$  then
12:      Extending:  $\mathcal{N}_t \leftarrow \mathcal{N}_t \cup \text{EXTEND}(\tilde{n})$ 
13:    end if
14:  end for
15: end for

```

Algorithm 2 Generate child nodes for dual control steps

function BRANCH(n, \mathcal{M}, K)

```

1: Initialize the set of child nodes:  $\mathcal{C} \leftarrow \emptyset$ 
2: for all  $M \leftarrow \mathcal{M}$  do
3:   Randomly sample a set  $\{\theta_1^{M,o}, \theta_2^{M,o}, \dots, \theta_K^{M,o}\}$ 
   from the standard Gaussian  $\mathcal{N}(0, I)$ 
4:   Randomly sample a set  $\{\bar{d}_1^{M,o}, \bar{d}_2^{M,o}, \dots, \bar{d}_K^{M,o}\}$ 
   from the standard Gaussian  $\mathcal{N}(0, I)$ 
5:   for all  $k \leftarrow 1, 2, \dots, K$  do
6:     Create a node  $\tilde{n}$ 
7:      $\theta_{\tilde{n}}^{M,o} = \theta_k^{M,o}, \bar{d}_{\tilde{n}}^{M,o} = \bar{d}_k^{M,o}, M_{\tilde{n}} = M$ 
8:      $t_{\tilde{n}} = t_n + 1$ 
9:      $\mathcal{C} \leftarrow \mathcal{C} \cup \{\tilde{n}\}$ 
10:  end for
11: end for
12: return  $\mathcal{C}$ 

```

Algorithm 3 Generate a child node for exploitation steps

function EXTEND(n)

```

1: Create a node  $\tilde{n}$ 
2:  $t_{\tilde{n}} = t_n + 1, \theta_{\tilde{n}}^{M,o} = 0, \bar{d}_{\tilde{n}}^{M,o} = 0, M_{\tilde{n}} = M_n$ 
3: return  $\{\tilde{n}\}$ 

```

as an implicit dual control method Mesbah (2018). Unlike conventional ST-SMPC methods in which uncertainty samples are fixed during optimization, such as Lucia et al. (2013); Schildbach and Borrelli (2015); Hu et al. (2022), our scenario tree has both *state- and input-dependent* uncertainty realizations, leading to a *dynamic* scenario tree. As a result, uncertainty samples can adjust their value in response to predicted states and inputs during online optimization. Fundamentally, it is this feature that allows the ego agent to interact with the opponent in a way that promotes the dual control effect, which is explained in detail in Theorem 1.

We denote a *node* in the scenario tree as n , whose time, state, and belief state are denoted as t_n, x_n , and b_n , respectively. Similarly, the uncertainty samples of the node are θ_n^M, \bar{d}_n^M , and M_n . Here, recall that \bar{d}_n^M is the combined disturbance defined in (10), which implicitly characterizes a sample of the opponent's action. The set of all nodes is defined as \mathcal{N} . We define the transition probability from a parent node $p(n)$ to its child node n as $\bar{P}_n := P(\theta_n^M | \mathcal{I}_{p(n)}; M_n)P(\bar{d}_n^M | \mathcal{I}_{p(n)}; M_n)P(M_n | \mathcal{I}_{p(n)})$. Subsequently, the *path transition probability* of node n , i.e. the transition probability from the root node n_0 to node n can be computed recursively as $P_n := \bar{P}_n \cdot \bar{P}_{p(n)} \cdots \bar{P}_{n_0}$, with $\bar{P}_{n_0} = 1$.

In order to quickly compute the conditional probabilities of $(\theta_n^M, \bar{d}_n^M)$ and avoid online sampling (i.e. during the optimization), we use an offline sampling procedure, leveraging the fact that they are (conditional) Gaussian random variables, similar to what is done in Arcari et al. (2020b); Bonzanini et al. (2020). We first generate samples offline from the standard Gaussian distribution. Then, during online optimization, these samples are transformed using the analytical mean and covariance expressions:

$$\theta_n^M = \mu^{\theta_n^M}(x_n, u_n^e) + \left(\Sigma^{\theta_n^M}(x_n, u_n^e) \right)^{1/2} \theta_n^{M,o}, \quad (14a)$$

$$\bar{d}_n^M = \left(\tilde{\Sigma}^{\bar{d}_n^M}(x_n, u_n^e) \right)^{1/2} \bar{d}_n^{M,o}. \quad (14b)$$

This reveals the dynamic nature of our proposed scenario tree: the uncertainty samples are adjustable during optimization via transformations (14a) and (14b); the path transition probabilities are also state- and input-dependent due to the Bayesian update of M in (3b). The scenario tree construction procedure is summarized in Alg. 1.

Remark 6. In order to alleviate the exponential growth of complexity associated with the scenario tree, only a small number of $\theta_n^{M,o}$, $\bar{d}_n^{M,o}$ and M are sampled. We developed a scenario pruning mechanism in our prior work Hu et al. (2022) for static scenario trees, which can be used here as a heuristic to prune branches based on the last optimized scenario tree. Principled pruning method for dynamic scenario trees involving state- and input-dependent uncertainty realizations remains an open question.

5.4 Exploitation Steps

In order to alleviate the computation challenge caused by the exponential growth of nodes in the scenario tree, we can stop branching the tree at a stage $N^d < N$, which we refer to as the dual control horizon. Subsequently, the remaining $N^e := N - N^d$ stages become the exploitation horizon, where each scenario is extended without branching and the belief states are only propagated with the transition dynamics $g^t(\cdot)$ defined in (3d), corresponding to a non-dual SMPC problem. Thanks to the scenario tree structure, control inputs of the exploitation steps still preserve the causal feedback property, allowing the robot to be cautious and “passively adaptive” to future opponent's uncertainty realizations.

6 Shielding-Aware Safe Dual Control

In this section, we revisit safety constraint (5e) and provide safety guarantees for the closed-loop system using the

proposed implicit dual SMPC policy. Our roadmap is as follows. First, to ensure that $x_t \notin \mathcal{F}$ for all $t \geq 0$ despite the *worst-case* opponent's actions and external disturbances[†], we use a class of least-restrictive supervisory control schemes, often referred to as *shielding*. Examples of shielding methods and applications of shielding for safe control include, but not limited to: Bansal et al. (2017); Fisac et al. (2018a); Bonzanini et al. (2020); Bastani (2021); Wabersich and Zeilinger (2021); Hu et al. (2022). This approach relies on a safety fallback policy, usually as the “last resort”, which overrides a nominal policy when a safety-critical event, e.g. a collision, is imminent. The *reactive* nature of a shielding policy makes it agnostic to ego's planning efficiency, and oftentimes conflicts with the probing actions generated by the dual control policy, leading to performance degradation in planning. To mitigate the conflict between safety overrides and active uncertainty reduction, we augment the implicit dual SMPC method developed in Section 5 with the recently proposed shielding-aware robust planning (SHARP) framework Hu et al. (2022). The key feature of SHARP is that it makes use of the propagated belief states to causally anticipate possible shielding events in the future, thereby *proactively* balancing the nominal planning performance with costly emergency maneuvers triggered by unlikely opponent's behaviors. The resulting policy ultimately leads to, instead of a low probability of collision, a low chance of having to apply the costly shielding policy. Note that the original SHARP framework in Hu et al. (2022) assumes that the opponent is oblivious to the ego agent. In the following, we will lift this overly conservative assumption and explicitly account for opponent's responses.

6.1 Shielding for Safe Interaction Planning

In this paper, we focus on providing robust (worst-case) safety guarantees for interaction planning. Therefore, we make an operational design domain (ODD) Lee et al. (2020) assumption that the external disturbance d_t is bounded.

Assumption 1. The external disturbance d_t is bounded element-wise, i.e. $d_t \in \mathcal{D} \subseteq \mathbb{R}^{n_x}$ and $\bar{d}_{\min}^i \leq d_t^i \leq \bar{d}_{\max}^i$ for all $i = 1, \dots, n_x$.

A *shielding mechanism* is defined as a tuple (Ω, π^s) , where set $\Omega \subseteq \mathbb{R}^{n_x}$ is a safe set that is *robust controlled-invariant* Blanchini (1999) and satisfies $\Omega \cap \mathcal{F} = \emptyset$, and $\pi^s : \mathbb{R}^{n_x} \rightarrow \mathcal{U}^e$ is a safe control policy that keeps the state of joint system (1) inside Ω even under the worst-case opponent's action and external disturbance.

Definition 2. Robust controlled-invariant set. Given joint dynamics (1) with bounded opponent's actions $u_t^o \in \mathcal{U}^o$ and uncertain input $d_t \in \mathcal{D}$, a set $\Omega \subseteq \mathbb{R}^{n_x}$ is a robust controlled-invariant set if there exists a control policy $\pi^s : \mathbb{R}^{n_x} \rightarrow \mathcal{U}^e$ that keeps x_t from leaving Ω :

$$x_0 \in \Omega \\ \Rightarrow x_t \in \Omega, \forall t > 0, \forall u_t^o \in \mathcal{U}^o, \forall d_t \in \mathcal{D}, u_t^e = \pi^s(x_t).$$

Let x^+ denote the next state evolved with (1) given x, u^e, \tilde{u}^o , and \tilde{d} , we subsequently define the *shielding set*:

$$\mathcal{S}^e = \{(x, u^e) \in \Omega \times \mathcal{U}^e \mid \exists \tilde{u}^o \in \mathcal{U}^o, \exists \tilde{d} \in \mathcal{U}^o : \\ x^+ \left(x, u^e, \tilde{u}^o, \tilde{d} \right) \notin \Omega\},$$

which contains all state-action pairs that *might* lead to the next state departing the safe set. Based on shielding mechanism (Ω, π^s) , we can then define a least-restrictive supervisory *safety filter* as a switching policy:

$$u_t^e = \pi^f(x_t; \tilde{u}_t^e) := \begin{cases} \tilde{u}_t^e, & \text{if } (x_t, \tilde{u}_t^e) \notin \mathcal{S}^e \\ \pi^s(x_t), & \text{if } (x_t, \tilde{u}_t^e) \in \mathcal{S}^e. \end{cases} \quad (15)$$

Safety filter (15) allows the ego agent to apply *any* nominal controller $\pi_t : \mathbb{R}^{n_x} \rightarrow \mathcal{U}^e$ as long as $(x_t, \pi_t(x_t))$ is not in the shielding set \mathcal{S}^e ; otherwise, it overrides $\pi_t(x_t)$ with the shielding policy $\pi^s(x_t)$. This leads to the following result.

Proposition 1. Safety Filter (Prop. 1 Hu et al. (2022)). If a set Ω is robust controlled-invariant under shielding policy $\pi^s(\cdot)$, then it is robust controlled-invariant under safety filter policy $\pi^f(\cdot; \pi_t(\cdot))$, for any nominal policy $\pi_t(\cdot)$.

Remark 7. We can replace (5e) with chance constraints to account for uncertain inputs with unbounded supports, i.e. $P[x \notin \mathcal{F}] \geq 1 - \delta$, where $\delta \in (0, 1]$ is the tolerance level. Then, probabilistic safety guarantees can be obtained via probabilistic shielding methods such as Bastani et al. (2021).

6.2 Interaction-Aware SHARP

In the SHARP framework, safety filter (15) is supplied with the predicted future states and opponent's actions along each branch of the scenario tree to *causally anticipate* possible future shielding events, therefore making the resulting policy aware of the (usually costly) shielding maneuvers. However, (15) involves conditioning on set inclusion relationships, making it hard to optimize within the SMPC problem. To this end, we modify and improve the approximate local safety filter scheme proposed in Hu et al. (2022) to reformulate (15) as a convex constraint, which additionally accounts for the opponent's responses and external disturbance.

We start by linearizing joint system (1) at a given nominal state $\bar{x}_{\tilde{n}}$ associated with node \tilde{n} :

$$\delta x_{\tilde{n}}^+ = A_{\tilde{n}} \delta x_{\tilde{n}} + B_{\tilde{n}}^e u_{\tilde{n}}^e + B_{\tilde{n}}^o u_{\tilde{n}}^o + d_{\tilde{n}}, \quad (16)$$

where $A_{\tilde{n}} := \nabla_x f(x)|_{\bar{x}_{\tilde{n}}}$, $B_{\tilde{n}}^e := B^e(\bar{x}_{\tilde{n}})$, $B_{\tilde{n}}^o := B^o(\bar{x}_{\tilde{n}})$, and $\delta x_{\tilde{n}} = x_{\tilde{n}} - \bar{x}_{\tilde{n}}$. Then, we approximate the safe set Ω as a halfspace locally at $x_{\tilde{n}}$:

$$\Omega_{\tilde{n}} = \{\delta x \mid H_{\tilde{n}}^\top \delta x \geq 0\}, \quad (17)$$

where $H_{\tilde{n}} := \bar{x}_{\tilde{n}}^\perp - \bar{x}_{\tilde{n}}$ approximates the normal vector of the tangent space of Ω at $x_{\tilde{n}}$, as illustrated in Figure 4. Now, given uncertain linear system (16) and halfspace safe set $\Omega_{\tilde{n}}$, we extend the result in Agrawal and Sreenath (2017) to construct an affine robust control barrier function (RCBF) constraint that approximates (15). This RCBF locally captures the shielding maneuver by inducing a constraint that certifies the controlled invariance of the approximate safe set $\Omega_{\tilde{n}}$, which is formalized in Lemma 2.

Definition 3. Discrete-Time Exponential RCBF. A map $h(x)$ is a discrete-time exponential robust control barrier function for system $x_{t+1} = f(x_t, u_t, d_t)$ if:

[†]This can also be interpreted as the maximal model mismatch when using (2) to predict the opponent's action and future state evolution.

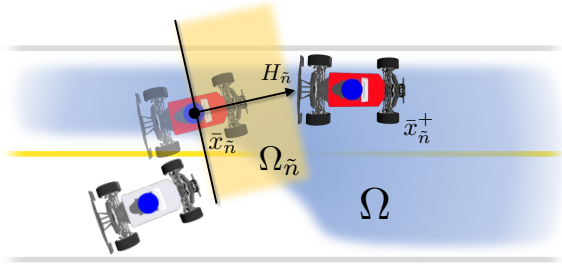


Figure 4. Illustration of an RCBF-based halfspace safe set $\Omega_{\tilde{n}}$ (yellow), which approximates safe set Ω (blue) locally at $x_{\tilde{n}}$.

(a) $h(x_0) \geq 0$ and,

(b) $\exists u_t \in \mathcal{U}$ such that $h(x_{t+1}) - h(x_t) + \gamma h(x_t) \geq 0$ for all $t \geq 0$, $d_t \in \mathcal{D}$, and some $\gamma \in (0, 1]$.

Lemma 2. Let Assumption 1 hold. For uncertain linear system (16), given an opponent's control $u^o \in \mathcal{U}^o$, set $\Omega_{\tilde{n}}$ define by (17) is robust controlled-invariant under policy $u_{\tilde{n}}^e \in \mathcal{U}^e$ if it satisfies:

$$H_{\tilde{n}}^\top [(A_{\tilde{n}} + (\gamma - 1)I) \delta x_{\tilde{n}} + B_{\tilde{n}}^e u^e + B_{\tilde{n}}^o u^o + d_{\tilde{n}}^*] \geq 0, \quad (18)$$

for all $\delta x \in \Omega_{\tilde{n}}$ and some $\gamma \in (0, 1]$. Here, the optimal (worst-case) disturbance $d_{\tilde{n}}^*$ is defined element-wise as:

$$d_{\tilde{n}}^{*,i} := \begin{cases} \bar{d}_{\min}^i, & \text{if } H_{\tilde{n}}^i \geq 0 \\ \bar{d}_{\max}^i, & \text{otherwise.} \end{cases} \quad (19)$$

The proof can be found in Appendix B.2. Condition (18) is affine (and hence convex) in $\delta x_{\tilde{n}}$ and u^e , and u^o , which is efficient to optimize and can be infused into the ST-SMPC problem as an inequality constraint for causal shielding anticipation. Instead of using the worst-case opponent's action in (18), we allow it to depend on the opponent's action u^o , which is a decision variable affected by the ego's action and state of the system. This enables SHARP to account for interaction while predicting future shielding events.

Remark 8. As pointed out in Agrawal and Sreenath (2017), it is not guaranteed that there exists a feasible solution to constraint (18) when the ego's control input is bounded. In order to ensure that the ST-SMPC problem is recursively feasible, we incorporate (18) as a soft constraint by adding a slack variable.

At time t , based on the last optimized scenario tree \mathcal{N}_{t-1}^* , we can perform a one-step simulation rollout per (15) to identify nodes at which the shielding policy shall be used. We denote the set of all shielding nodes at time t as \mathcal{N}_t^s . The convex shielding-aware constraint (18) is enforced for all $\tilde{n}^s \in \mathcal{N}_t^s$. The procedure of finding \mathcal{N}_t^s is summarized in Algorithm 4.

6.3 Overall Algorithmic Approach

Given the current state measurement \hat{x}_t , the last updated belief state \hat{b}_t , and a scenario tree defined by node sets \mathcal{N}_t , we can reformulate (5) as an ST-SMPC problem in a similar

Algorithm 4 Identify shielding nodes

Input: Last optimized scenario tree defined by node set \mathcal{N}_{t-1}^* , scenario tree defined by node set \mathcal{N}_t
Output: Shielding node set \mathcal{N}_t^s

- 1: Initialize the shielding node set: $\mathcal{N}_t^s \leftarrow \emptyset$
- 2: **for all** $(\tilde{n}^*, \tilde{n}) \leftarrow \text{zip}(\mathcal{N}_{t-1}^*, \mathcal{N}_t)$ **do**
- 3: $\tilde{x}_{\tilde{n}}^+ \leftarrow$ one-step forward simulation using $x_{\tilde{n}}^*$, $u_{\tilde{n}}^e$, $u_{\tilde{n}}^o$, $\bar{d}_{\tilde{n}}^M$ and dynamics (20c)
- 4: **if** $\tilde{x}_{\tilde{n}}^+ \notin \Omega$ **then**
- 5: Compute $H_{\tilde{n}}$, $A_{\tilde{n}}$, $B_{\tilde{n}}^e$, $B_{\tilde{n}}^o$, and $d_{\tilde{n}}^*$ according to Section 6.2
- 6: $\mathcal{N}_t^s \leftarrow \mathcal{N}_t^s \cup \{\tilde{n}\}$
- 7: **end if**
- 8: **end for**

format to Bernardini and Bemporad (2011):

$$\min_{\mathbf{U}_t^e} \sum_{\tilde{n} \in \mathcal{N}_t \setminus \mathcal{L}_t} P_{\tilde{n}} \ell(x_{\tilde{n}}, u_{\tilde{n}}^e) + \sum_{\tilde{n} \in \mathcal{L}_t} P_{\tilde{n}} \ell_F(x_{\tilde{n}}) \quad (20a)$$

$$\text{s.t. } x_{n_0} = \hat{x}_t, b_{n_0} = \hat{b}_t, \quad (20b)$$

$$x_{\tilde{n}} = f(x_{p(\tilde{n})}) + B^o(x_{p(\tilde{n})})u_{\tilde{n}}^o(x_{p(\tilde{n})}, u_{p(\tilde{n})}^e) + B^e(x_{p(\tilde{n})})u_{p(\tilde{n})}^e + \bar{d}_{\tilde{n}}^M, \quad \forall \tilde{n} \in \mathcal{N}_t \setminus \{n_0\} \quad (20c)$$

$$b_{\tilde{n}} = \tilde{g}(b_{p(\tilde{n})}, x_{\tilde{n}}, u_{p(\tilde{n})}^e), \quad \forall \tilde{n} \in \mathcal{N}_t^d \quad (20d)$$

$$b_{\tilde{n}} = g^t(b_{p(\tilde{n})}), \quad \forall \tilde{n} \in \mathcal{N}_t^e \quad (20e)$$

$$u_{\tilde{n}}^e \in \mathcal{U}^e, u_{\tilde{n}}^o \in \mathcal{U}^o, \quad \forall \tilde{n} \in \mathcal{N}_t \setminus \mathcal{L}_t \quad (20f)$$

$$(18), \quad \forall \tilde{n} \in \mathcal{N}_t^s \quad (20g)$$

where \mathcal{L}_t is the set of all leaf nodes, (i.e. ones that do not have a descendant), \mathcal{N}_t^d and \mathcal{N}_t^e are the set of dual control and exploitation nodes, respectively, set $\mathbf{U}_t^e := \{u_{\tilde{n}}^e \in \mathbb{R}^{m_e} : \tilde{n} \in \mathcal{N}_t \setminus \mathcal{L}_t\}$ is the collection of the ego's control inputs associated with all non-leaf nodes, and \mathcal{N}_t^s is shielding node set returned by Algorithm 4, containing nodes at which the convex shielding-aware constraint (18) is imposed. Objective function (20a) approximates (5a) based on uncertainty samples of the scenario tree. Constraints (20b)-(20g) capture the initial (belief) state, dynamics of the physical states, belief dynamics of the exploration and exploitation steps, control limits, and convex shielding-aware constraints, respectively. Problem (20) is a nonconvex trajectory optimization problem, which can be solved using general-purpose nonconvex solvers such as SNOPT Gill et al. (2005) and IPOPT Wächter and Biegler (2006). The optimal solution $\mathbf{U}_{t^*}^e$ to (20) is implemented in a receding horizon fashion, i.e. $\pi_{\text{IDSMPC-SHARP}}^e(\hat{x}_t, \hat{b}_t) := u_{n_0}^{e,*}$, and we refer to this as the shielding-aware implicit dual SMPC (IDSMPC-SHARP) policy. Our overall algorithmic approach, which is centered around the IDSMPC-SHARP policy, can be found in Algorithm 5.

Remark 9. When cost functions in (20a) are quadratic, i.e. $\ell(x, u) = \|x\|_Q^2 + \|u\|_R^2$ and $\ell_F(x) = \|x\|_{Q_F}^2$, an approximation technique can be deployed to analytically evaluate the expected cost with respect to the state. Let $A_{p(\tilde{n})}$ denote the Jacobian of dynamics (20c) evaluated at the mean value of state $\mu_{p(\tilde{n})}^x$ and ego's control $u_{p(\tilde{n})}^e$. Then, the state will remain Gaussian-distributed along each branch in

the scenario tree, whose covariance is given by the recursive formula: $\Sigma_{\tilde{n}}^x = \Sigma_{\tilde{n}}^{\bar{d}}(\mu_{\mathbf{p}(\tilde{n})}^x, u_{\mathbf{p}(\tilde{n})}^e) + A_{\mathbf{p}(\tilde{n})} \Sigma_{\mathbf{p}(\tilde{n})}^x A_{\mathbf{p}(\tilde{n})}^\top$. We recall that $\mathbb{E}_{\xi \sim \mathcal{N}(0, I)} [(W\xi)^\top Q(W\xi)] = \text{tr}(W^\top QW)$. Therefore, objective (20a) can be approximated as

$$\sum_{\tilde{n} \in \mathcal{N}_t \setminus \mathcal{L}_t} P_{\tilde{n}} \ell(x_{\tilde{n}}, u_{\tilde{n}}^e) + \sum_{\tilde{n} \in \mathcal{L}_t} P_{\tilde{n}} \ell_F(x_{\tilde{n}}) + \sum_{\tilde{n} \in \mathcal{N}_t} \text{tr}(Q \Sigma_{\tilde{n}}^x)$$

where the path transition probability of node \tilde{n} evaluates to $P_{\tilde{n}} = P(\theta_{\tilde{n}}^M | \mathcal{I}_{\mathbf{p}(\tilde{n})}; M_n) P(M_n | \mathcal{I}_{\mathbf{p}(\tilde{n})}) P_{\mathbf{p}(\tilde{n})}$. This way, only the hidden states are sampled for computing the expected cost, and no \bar{d}^M sample is needed.

Algorithm 5 Shielding-aware safe dual control

Input: Initial state x_0 , initial belief state b_0 , Q-value functions $Q_i^M(\cdot)$ in (2), shielding mechanism (Ω, π^s)

- 1: Initialization: $t \leftarrow 0, \mathcal{N}_0^* \leftarrow \emptyset$
- 2: **while** Planning goal is not reached **do**
// Planning:
 - 3: $\mathcal{N}_t \leftarrow$ construct a scenario tree using Algorithm 1
 - 4: $\mathcal{N}_t^s \leftarrow$ identify the shielding nodes and construct shielding-aware constraints using Algorithm 4
 - 5: $\pi_{\text{IDSMPC-SHARP}}^e(x_t, b_t), \mathcal{N}_t^* \leftarrow$ solve ST-SMPC (20)
 - // Shielding:
 - 6: Apply safety filter policy (15) to the ego agent: $u_t^e = \pi^f(x_t; \pi_{\text{IDSMPC-SHARP}}^e(x_t, b_t))$
 - // Belief Update:
 - 7: Measure new state x_{t+1}
 - 8: $b_{t+1} \leftarrow$ update belief states using (3a)-(3d)
 - 9: Update time: $t \leftarrow t + 1$
- 10: **end while**

6.4 Properties of the Planning Framework

In this section, we examine the properties of the proposed IDSMPC-SHARP control policy, as well as the behavior of the joint system (1) in closed-loop with Algorithm 5.

Theorem 1. Dual Control Effect. *The feedback control policy $\pi_{\text{IDSMPC-SHARP}}^e(\cdot, \cdot)$ obtained by solving (20) produces dual control effect.*

Proof. From Lemma 1, for any given time $t \geq 0$, the robot's control u_t^e can affect $\Sigma_{t+1}^{\theta^M}$, the covariance (second-order moment) of the belief over θ^M . Therefore, the policy $\pi_{\text{IDSMPC-SHARP}}^e$ produces dual control effect for hidden state θ^M per Definition 1(a). We recall the measurement update equation for the categorical belief over M from (3b):

$$p(M_- | \mathcal{I}_{t+1}) = \frac{p(x_{t+1} | u_t^e, \mathcal{I}_t; M) p(M | \mathcal{I}_t)}{p(x_{t+1} | u_t^e, \mathcal{I}_t)},$$

which shows that the ego's control u_t^e can affect all components of the categorical distribution over M , and thereby its entropy:

$$H(M_- | \mathcal{I}_{t+1}) \propto \sum_{\tilde{M} \in \mathcal{M}} P(\tilde{M} | \mathcal{I}_{t+1}) \log P(\tilde{M} | \mathcal{I}_{t+1}),$$

implying dual control effect for M per Definition 1(b). \square

Remark 10. Optimality. *The solution to ST-SMPC (20) is in general sub-optimal with respect to Bellman recursion (6) due to the approximate belief state dynamics \tilde{g} , expected cost approximated with uncertainty samples, truncated exploration steps, and that the solution to the nonconvex program (20) is oftentimes only locally optimal. Therefore, the optimal exploration-exploitation trade-off is generally not achieved. Nonetheless, since the ego's control produces dual control effect for the hidden states per Theorem 1, it thereby automatically balances the nominal planning performance and uncertainty reduction, to the extent that local optimality of (20) is achieved.*

Remark 11. Guaranteed Feasibility. *ST-SMPC problem (20) is guaranteed to be feasible since the convex shielding-aware constraint (18) is enforced as a soft constraint per Remark 8.*

Theorem 2. Recursive Safety. *Suppose the initial state is in the safe set, i.e. $x_0 \in \Omega$, then the joint system (1) in closed-loop with Algorithm 5 remains safe, i.e. $x_t \in \Omega, \forall t > 0$.*

Proof. The result is a direct consequence of Proposition 1 and Definition 2. \square

7 Simulation Studies

7.1 Simulation Setup

We evaluate our proposed implicit dual scenario tree-based SMPC (IDSMPC) and IDSMPC-SHARP planners on simulated driving scenarios. In both planning and simulation, vehicle and pedestrian dynamics are described by the 4D kinematic bicycle model in Zhang et al. (2020) and the 4D unicycle model in Fridovich-Keil et al. (2020), respectively, both discretized with a time step of $\Delta t = 0.2$ s. All simulations are performed using MATLAB and YALMIP Löfberg (2004) on a desktop with an Intel Core i7-10700K CPU. All nonlinear MPC problems are solved with SNOPT Gill et al. (2005). Parameter values used for simulation can be found in Table 2. The open-source code is available online.[‡]

7.1.1 Baselines. We compare our proposed IDSMPC and IDSMPC-SHARP planners against four baselines:

- Explicit dual SMPC (EDSMPC), which augments the stage cost ℓ in (5a) with an information gain term $\lambda(H(b_k) - H(b_{k+1}))$ proposed by Sadigh et al. (2018), leading to an explicit dual stochastic optimal control problem. Here, $\lambda > 0$ is a fine-tuned weighting factor. Similar to IDSMPC, the expected cost is also computed approximately using uncertainty samples.
- Non-dual scenario-based SMPC (NDSMPC), which is based on solving (5) with a scenario tree that does not propagate belief states with the measurement update (20d) (so the resulting policy does not have dual control effect). A similar scenario program can also be found in Bernardini and Bemporad (2011); Schildbach and Borrelli (2015); Hu et al. (2022).

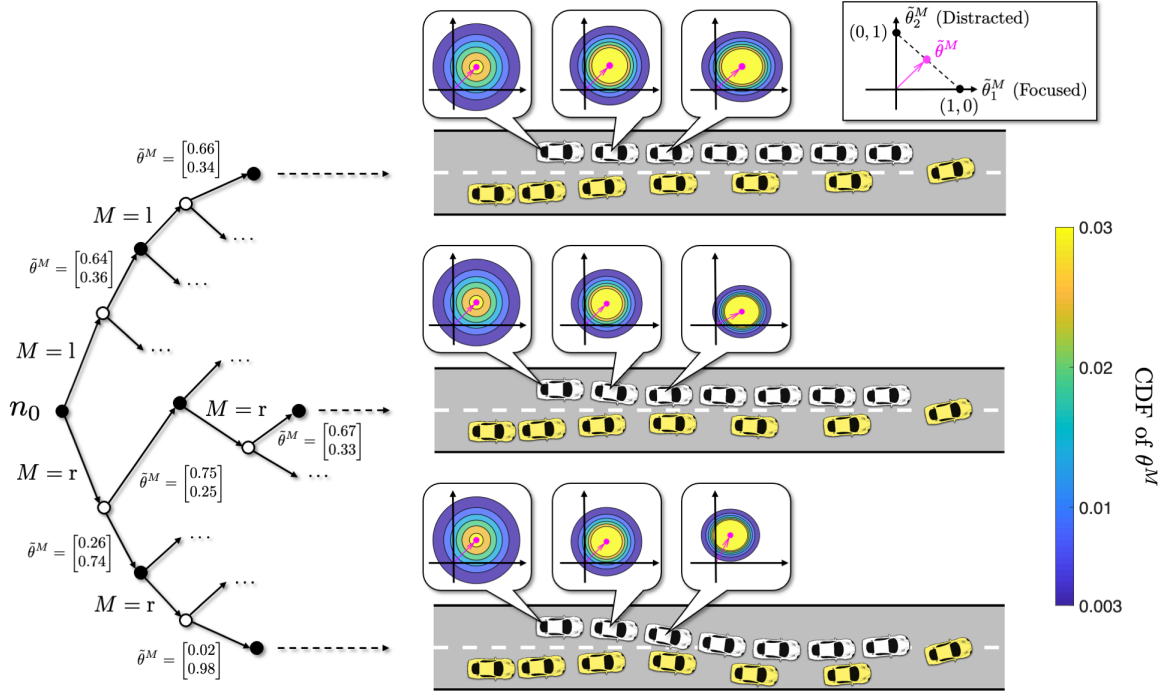


Figure 5. Illustration of a scenario tree and the resulting optimized scenario trajectories with $N^d = 2$ dual control time steps and $N^e = 4$ exploitation steps for the highway overtaking example in Section 7.2.2. The human-driven vehicle and autonomous car are plotted in white and yellow, respectively. Hidden state θ^M is modeled as a 2D Gaussian random variable, which is normalized to a 1-simplex for visualization. The magenta arrows show the MAP mean of the normalized hidden state $\tilde{\theta}^M$. The contour plots display level sets of the cumulative distribution function (CDF) of θ^M . Uncertainty is less significantly reduced in the case where the human prefers the left lane (upper branch) since their behavior is less influenced by the robot's (probing) actions than in the right lane case.

- Certainty-equivalent MPC (CEMPC), which is based on solving (5) with the certainty-equivalence principle Mesbah (2018); Arcari et al. (2020a). The maximum a posteriori (MAP) strategy alignment method Peters et al. (2020) is used by the ego agent to modify the planning problem, e.g. in Example 1, if both the ego and opponent vehicles drive on the inner lane, and the MAP estimate of M is NY (not yielding), then the reference lane of the ego would be set to the outer lane (by modifying costs $\ell(\cdot)$ and $\ell_F(\cdot)$) so that it can safely overtake the opponent.
- Iterative linear-quadratic game with inference-based strategy alignment (ISA-iLQ), proposed by Peters et al. (2020) and originally developed in Fridovich-Keil et al. (2020). An input projector is used to enforce $u^o \in \mathcal{U}^o$ and $u^e \in \mathcal{U}^e$.

EDSMPC is a dual control planner while the other three do not generate dual control effect. All planners use the same quadratic cost functions ℓ and ℓ_F for penalizing reference tracking error and control magnitude, and are equipped with the same Bayesian-inference-based opponent intent inference scheme. To incrementally interpret the results, IDSMPC and four baselines are unshielded and, to account for safety, we use the soft constrained MPC approach in Zeilinger et al. (2014), which relaxes the original hard constraints $x_{\tilde{n}} \notin \mathcal{F}$ with slack variables for each node $\tilde{n} \in \mathcal{N}_t$, making those planners *safety-aware but shielding-agnostic*. IDSMPC-SHARP uses a shielding mechanism given by a contingency planner design Hardy and Campbell (2013); Bajcsy et al. (2021) that safeguards

against the opponent's behavioral uncertainties and external disturbances (under Assumption 1). The contingency planning problem was solved online with the iterative Linear-Quadratic Regulator (iLQR) method Todorov and Li (2005). We use the model predictive shielding (MPS) algorithm Bastani (2021) to ensure recursive feasibility of the shielding policy.

7.1.2 Metrics. To measure the planning performance, we consider the following two metrics:

- Closed-loop cost, defined as $J_{cl}^e := \sum_{t=0}^{T_{sim}} \ell(x_t, u_t^e)$, where T_{sim} is the simulation horizon, and $x_{[0:T_{sim}]}$, $u_{[0:T_{sim}]}$ are the *executed* trajectories (with replanning).
- Collision rate, defined as $N_{coll}/N_{trial} \times 100\%$, where N_{coll} is the number of trials that a collision happens, i.e. $x_t \in \mathcal{F}$, and N_{trial} is the total number of trials.

7.1.3 Hypotheses. We make four hypotheses, which are supported by our simulation results.

- **H1 (Performance and Safety Trade-off).** Dual control planners result in a better performance-safety trade-off than non-dual baselines.
- **H2 (Implicit vs Explicit Dual Control).** Explicit dual control is less efficient than its implicit counterpart, even with fine tuning.
- **H3 (Improved efficiency with SHARP).** Planning efficiency is improved using IDSMPC-SHARP compared to that of IDSMPC, even fine-tuned for safety.

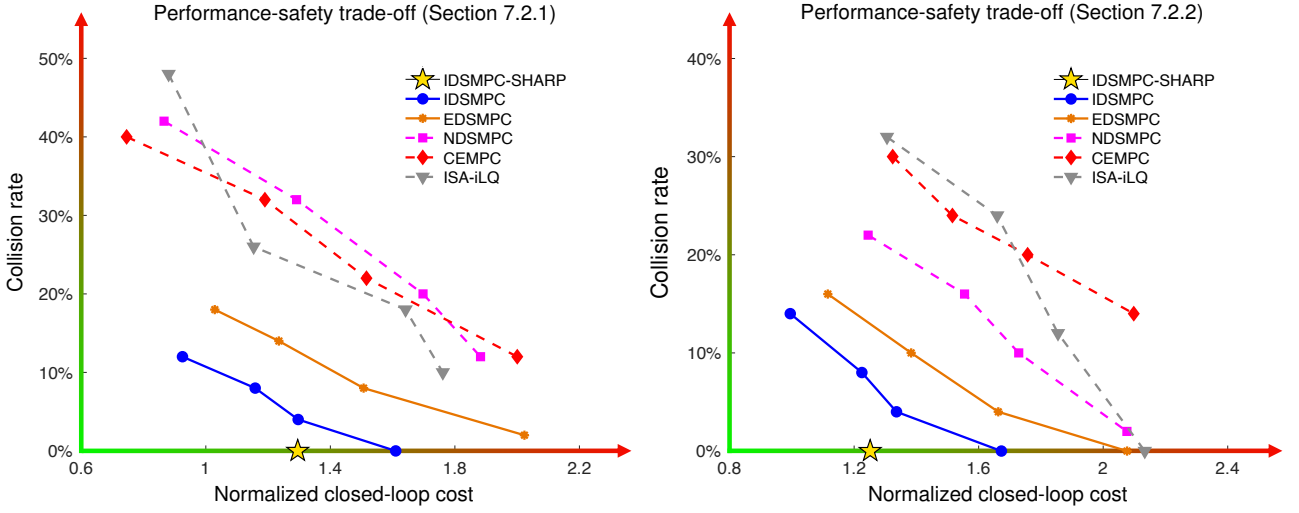


Figure 6. Performance-safety trade-off of simulation examples in Section 7.2.2 and 7.2.3. Closed-loop cost J_{cl}^e is normalized by 1×10^4 . For the unshielded planners (IDSMPC, EDSMPC, NDSMPC, CEMPC, and ISA-iLQ), each data point is obtained based on a distinct set of safety-critical tuning parameters of 50 trials with different random seeds. The data point associated with 50 simulation trials using IDSMPC-SHARP is shown in a yellow star. Curves of the dual control policies are shown as solid lines while those of the non-dual ones are shown as dashed lines. IDSMPC outperforms all baselines in terms of overall performance-safety trade-off. Due to shielding and the SHARP framework, IDSMPC-SHARP yields zero collision rate and about 20% less cost compared to the safest IDSMPC design.

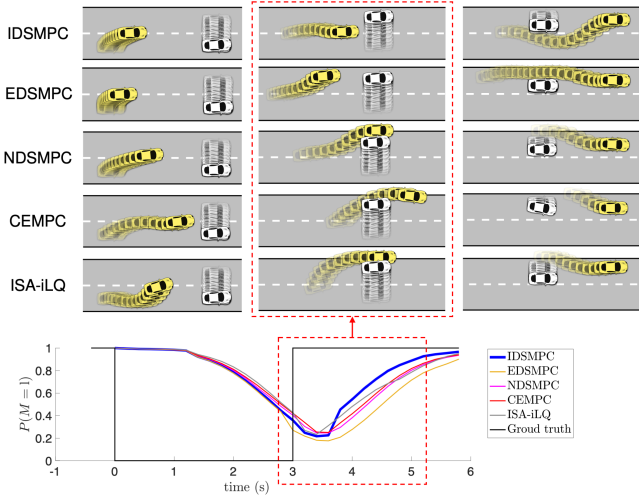


Figure 7. Simulation snapshots of Example 1. Longitudinal positions are shown in relative coordinates with $p_x^H = 0$. The left, middle, and right columns display trajectories for $t = [0, 3]$ s, $t = [3, 5]$ s, and the remainder of the trajectories. The bottom figure shows $P(M = 1)$ for all four planners over time. Our proposed IDSMPC planner yielded a clean and safe overtaking maneuver of the robot while the non-dual planners led to unsafe trajectories. When the robot is using EDSMPC, it stuck in a narrow window left to the human-driven car, resulting in a less efficient trajectory.

7.2 Simulated Opponent

7.2.1 Opponent's Policy. To show the efficacy of our method in general interaction planning settings, we produce the opponent agent's motion using an optimization-based simulator similar to [Baseggio et al. \(2011\)](#); [Guo et al. \(2013\)](#). The design parameters of the simulator are not accessible to the ego agent. While we have made our best effort to produce plausible simulated human agent behaviors that do not fall into the hypotheses captured by the motion prediction model

used by ST-SMPC (20), we acknowledge that our simulated human behavior might still differ from real-world human data, which are usually expensive and difficult to obtain, especially in an interactive setting. Nonetheless, we show in Section 7.3 an example where the human's trajectories are from the Waymo Open Motion Dataset [Sun et al. \(2020\)](#).

7.2.2 Objective and Awareness Uncertainty. Consider a highway driving scenario depicted in Figure 7, involving an autonomous vehicle (ego) and a human-driven vehicle (opponent). The continuous hidden state is defined as $\theta^M := (\theta_D^M, \theta_F^M)$ where θ_D^M and θ_F^M capture the level of distraction and focus of the human, respectively. A focused human accounts for the safety of the joint system (e.g. avoiding and making room for the robot when it attempts to merge in front of the human), while a distracted human does not. The discrete hidden state M models if the human prefers to drive in the left lane or in the right lane, i.e. $M \in \{l, r\}$. An optimized scenario tree of this example obtained by solving IDSMPC is visualized in Figure 5.

The performance-safety trade-off curve plotted in Figure 6 validates H1. Here, we design each *unshielded* planner with a set of fine-tuned safety-critical parameters, e.g. weight of the soft-constrained collision avoidance cost, robust margin of the failure set, and acceleration limits. For a given planner design, we simulate the scenario 50 times, each with a different random seed, which affects uncertainty sources including the initial conditions, additive disturbances, human's lane preference, and safety awareness. These random variables are independent of the (closed-loop) interactions between the human and the robot. Note that even the least conservative IDSMPC policy still leads to a lower collision rate than the baselines, and yields a closed-loop cost similar to those of non-dual policies. Although the EDSMPC policy also manages to achieve a low collision rate thanks to its ability to actively reduce human uncertainty, its overall closed-loop performance is consistently inferior

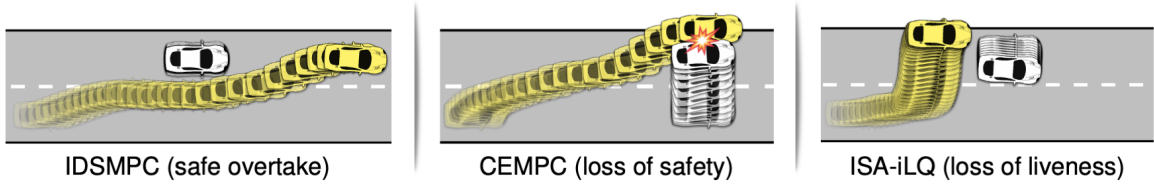


Figure 8. One trial of the highway driving example in Section 7.2.2. The left figure shows that the robot successfully overtook the human-driven vehicle in 6 s using IDSMPC. The middle and right figures display an unsafe trajectory for $t = [0, 4.6]$ s using CEMPC, and a trajectory generated where the robot failed to overtake the human in 10 s using ISA-iLQ, respectively.

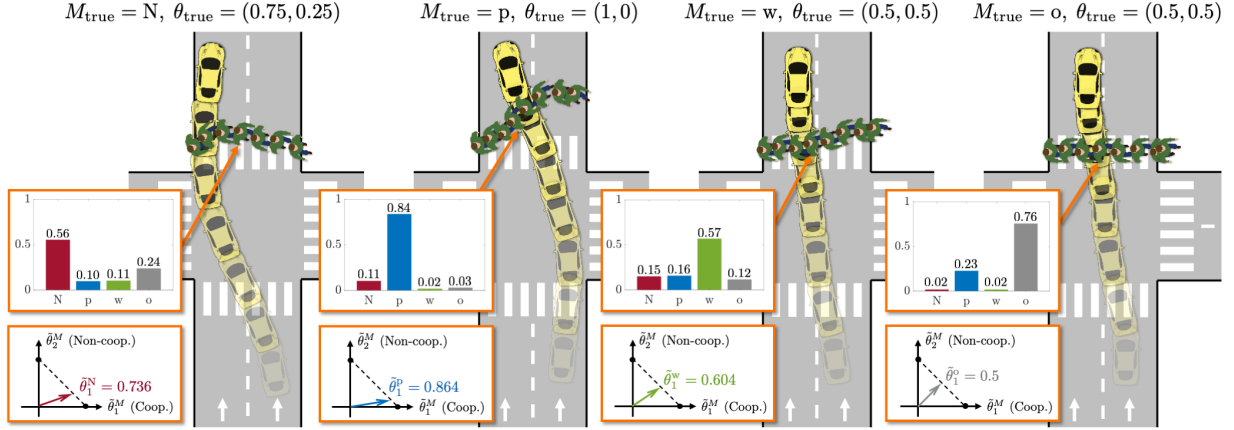


Figure 9. Simulation snapshots of Example 2 using the proposed IDSMPC planner. The human's mode is fixed throughout the simulation. In the orange blocks we display at $t = 2.6$ s the robot's running belief $p(M | \mathcal{I}_t)$ and $\hat{\theta}^M$, which is the MAP mean of θ^M normalized to a 1-simplex. The robot was able to quickly identify the human's hidden states and planned a collision-free trajectory in all four trials, accounting for the anticipated uncertainty reduction and interactions with the human.

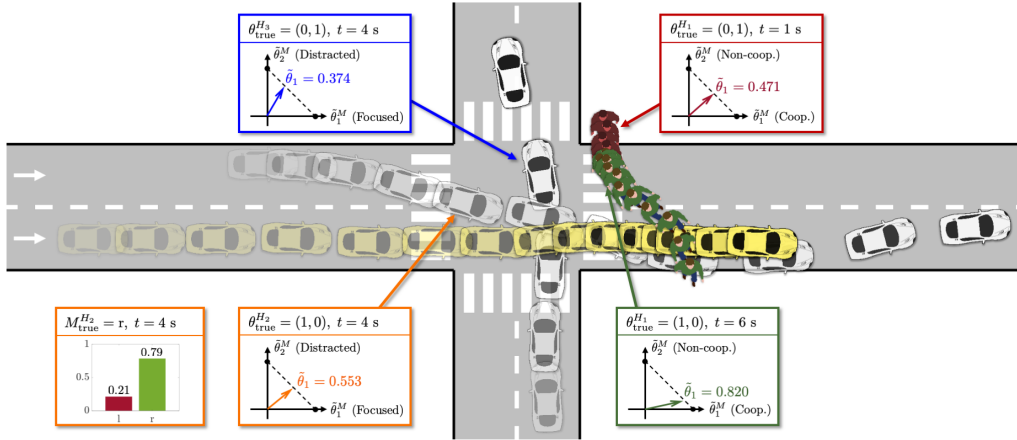


Figure 10. Simulation snapshots and estimated hidden states of a multi-agent interaction scenario with a pedestrian (H_1) and two human-driven vehicles (H_2 and H_3) using the IDSMPC planner. In the boxes we display at $t = 4$ s the continuous hidden state estimate $\hat{\theta}^M$ (normalized to a 1-simplex) of each opponent. For H_2 we also show the robot's running belief $p(M^{H_2} | \mathcal{I}_t)$.

to that of IDSMPC, which validates H2. Finally, we test IDSMPC-SHARP under the 50 scenarios governed by the same sequence of random seeds. Thanks to shielding, safety is assured for all 50 trials and, due to shielding awareness, the (normalized) average closed-loop cost (1.30) achieved by IDSMPC-SHARP is reduced by about 19% compared to that of IDSMPC (1.61), which is fine-tuned to achieve zero collision rate. This validates H3.

Trajectory snapshots and evolution of $P(M = 1)$ of one simulation trial are shown in Figure 7. The ground truth human's lane preference is the right lane for the first 3 s and then becomes the left lane for the remainder of the simulation, as shown at the bottom of Figure 7. The priors

are chosen as $P(M = 1) = 1$ and $\theta^1, \theta^r \sim \mathcal{N}((0.5, 0.5), 5I)$. Unlike non-dual control planners, IDSMPC controlled the robot to approach the human-driven vehicle along the center of the road, allowing the robot to informatively probe the human—which resulted in a more accurate prediction of M (bottom)—and guiding the robot through a region from which collisions can be avoided more easily. Indeed, as the human's hidden state M switched from r to l at $t = 6$ s, the robot using IDSMPC executed a sharp right turn and successfully avoided colliding with the human. The IDSMPC planner, although effective at reducing the uncertainty at the beginning, failed to recognize that overtaking the human from the right would have resulted

in a more efficient trajectory. All non-dual control planners, *even with replanning*, caused a collision with the human due to insufficient knowledge about M . It is also worth noticing that even if IDSMPC uses NDSMPC solutions for initialization, their closed-loop behaviors are vastly different, which essentially comes from the dual control effect.

In Figure 8, we examine another simulation trial. Using IDSMPC, the robot was able to safely overtake the human-driven car in 6 s. However, using the ISA-iLQ planner, the robot failed to overtake the human within 10 s. Due to lack of dual control effort, the robot was stuck behind the human, unaware of the human’s willingness to make room for the robot. Figure 8 also shows an unsafe trajectory generated with the CEMPC planner. Those results demonstrate that with dual control effort, the robot gains better *safety and liveness* when interacting with the opponent.

7.2.3 Behavioral and Cooperative Uncertainty. We next consider the uncontrolled traffic intersection scenario with the human uncertainty introduced in Example 2. Trajectory snapshots of four simulation trials using IDSMPC with different hidden states are shown in Figure 9. We chose uninformative prior distributions $p(M | \mathcal{I}_0) = [0.25 \ 0.25 \ 0.25 \ 0.25]$ and $\theta^M \sim \mathcal{N}((0.5, 0.5), 5I)$ for all $M \in \mathcal{M}$. We see that all four trials were safe and both the autonomous vehicle and pedestrian reached their target. The performance-safety trade-off curve is plotted in Figure 6 obtained based on 50 simulated trials, similar to Section 7.2.2. Again, we see that the IDSMPC policy leads to the best performance-safety trade-off among all unshielded planners, and a collision rate consistently lower than 15%. Safety is achieved for all trials with the shielded IDSMPC-SHARP policy, resulting in a (normalized) average closed-loop cost (1.25), which is 25% lower than what is achieved by the safest IDSMPC design (1.67).

7.2.4 Four-Agent Interaction Example. Finally, we apply IDSMPC to the same traffic intersection scenario as in Example 2 involving three human agents: two human-driven vehicles and a pedestrian. Human-driven vehicles are modeled with the objective and awareness uncertainty (Section 7.2.2), and the pedestrian is modeled with the behavioral and cooperative uncertainty (Example 2 and Section 7.2.3). In addition, we set up the simulation so that the pedestrian ignores other agents ($M = o$) for the first 2 s and then becomes safety-aware ($M = p$) for the remainder of the simulation. Trajectory snapshots of one representative trial are shown in Figure 10. The autonomous vehicle was able to quickly reduce the uncertainty of other agents and safely passed the traffic intersection.

7.3 Evaluation on the Waymo Motion Dataset

In this section, we provide additional simulation results for the highway driving scenario (Section 7.2.2), where the human driver’s trajectories are taken from the Waymo Open Motion Dataset [Sun et al. \(2020\)](#). We filtered out 50 trajectory data with different human motions and target lanes from the original dataset. Since the motion of the human-driven vehicle is generated by replaying the trajectory data, the human can be seen as completely unaware of safety, which is unknown to the robot. Statistical data of the closed-loop costs (normalized by 1×10^4) obtained from 50 trials

are plotted in Fig. 11, where all planners are shielded and thus all trials are safe. The (normalized) average closed-loop cost of IDSMPC-SHARP, IDSMPC, EDSMPC, NDSMPC, CEMPC, and ISA-iLQ are 1.09, 1.35, 1.57, 1.81, 1.89, and 1.86, respectively, as indicated by the central marks of the boxes in Fig. 11. Even if the human is unresponsive, dual control planners are still more efficient than non-dual ones due to active uncertainty reduction. IDSMPC-SHARP outperforms all other planners, showing its applicability under realistic interaction scenarios.

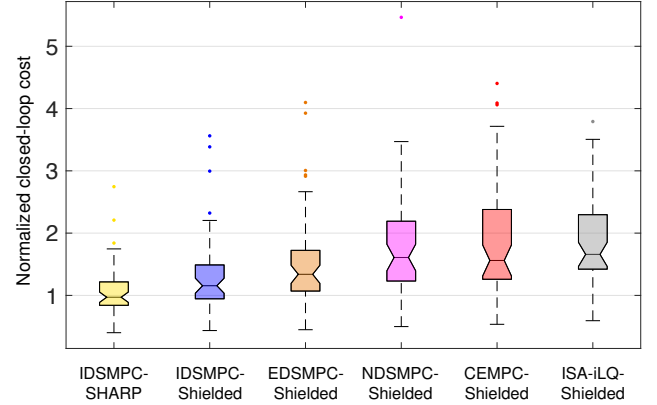


Figure 11. Closed-loop cost (normalized by 1×10^4) of the highway driving scenario (Section 7.2.2) with 50 realistic human-driven vehicle trajectories selected from the Waymo Open Motion Dataset [Sun et al. \(2020\)](#). Central marks, bottom, and top edges of the boxes indicate the median, 25th, and 75th percentiles, respectively. The maximum whisker length is set to 1.5, which leads to 99.3% coverage if the data are normally distributed. Outliers are shown as points.

8 Hardware Demonstration

8.1 Experiment Setup

In this section, we demonstrate our proposed IDSMPC-SHARP planning framework (Section 6) on Example 1 (overtaking) with two customized 1/10 scale Multi-agent System for non-Holonomic Racing (MuSHR) [Srinivasa et al. \(2019\)](#) autonomous vehicles (one ego and one opponent vehicle) at a test track of Honda Research Institute USA, Inc. in San Jose, CA. The 2D map of the track can be found in Figure 14. We use the Robot Operating System (ROS) to establish communications among sensors, actuators, and computing units. Each MuSHR robot (Figure 12) uses a LiDAR for determining its own state (position, velocity, and orientation) based on a given grid map of the track and surrounding landmarks, and communicates its *current* state with the opponent vehicle. The IDSMPC-SHARP and all comparative planners run at 10Hz on an Intel Xeon desktop with an E5-2640 CPU and send to the MuSHR vehicle the planned trajectory, which is tracked by a PID-based low-level controller running on an Intel NUC mini PC onboard MuSHR. Both the desktop and NUC run the Ubuntu 20.04 LTS operating system. We use the 4D kinematic bicycle model in [Zhang et al. \(2020\)](#) as the vehicle dynamics in both the ego’s and opponent’s MPC problem. All MPC problems in this section are modeled as nonlinear programs (NLPs) with CasADi [Andersson et al. \(2019\)](#) in Python and solved

in real time using IPOPT Wächter and Biegler (2006) with the linear system solving subroutine MA57 Duff (2004). We used HJ Reachability Bansal et al. (2017); Leung et al. (2020) to synthesize the shielding mechanism. The HJ-based shielding policy is pre-computed with OptimizedDP Bui et al. (2022) and deployed onboard Intel NUC. Parameter values used for hardware experiments can be found in Table 3 in Appendix A.2.



Figure 12. The MuSHR autonomous vehicle equipped with a LiDAR for localization.

8.1.1 Comparative Methods. We compare our proposed IDSMPC-SHARP planner against four other planners in hardware experiments:

- **“God’s planner”:** Oracle MPC, which computes the policy based on the opponent’s *communicated plans* computed at the current time.
- **Ablation I:** IDSMPC, which removes the shielding-aware constraint (18) from the SMPC problem (20), making it shielding-agnostic.
- **Ablation II:** NDSMPC-SHARP, which removes the belief dynamics (measurement update) (20d) and only updates the belief states with transition model (20e). The policy therefore passively reduces the uncertainty.
- **Baseline:** CEMPC-SHARP, which integrates the CEMPC planner introduced in Section 7.1 with the shielding-aware constraint (18).

Here, only the IDSMPC policy produces dual control effect among all four comparative methods. All planners use the same quadratic cost functions ℓ and ℓ_F , and are equipped with the same HJ-Reachability-based shielding mechanism.

8.1.2 Safety Regulations and Performance Metrics. Due to the relatively large size of the vehicle (approx. 40cm in width) compared to the lane width (approx. 60cm), we thereby define a trial to be *safe* if both of the following two regulations are satisfied:

- **SR1:** The ego and opponent vehicles do not collide (i.e. in physical contact) with each other, and
- **SR2:** At least one wheel of the ego vehicle is touching or inside the track limit (shown as the outer grey lines in Figure 14).

This safety regulation is motivated by typical car races, in which, similar to our case, vehicles are allowed to make aggressive overtaking maneuvers on relatively narrow lanes.

Motivated by Leung et al. (2020), we consider the following two metrics that evaluate the trade-off between safety and efficiency:

- **Safety index,** defined as

$$SI := \sum_{k=0}^{T_{\text{exp}}} \mathbf{1}[\ell_{\text{HJ}}(x_k) \geq 0] \ell_{\text{HJ}}(x_k),$$

where $T_{\text{exp}} > 0$ is the total number of time steps of an experiment trial and $\ell_{\text{HJ}}(\cdot)$ is the running cost (signed distance function Bansal et al. (2017)) used in HJ Reachability computation, which captures the penalty of violating safety regulations SR1 and SR2. This index captures the time-accumulated severity of safety violations (with respect to the shielding safe set Ω).

- **Efficiency index,** defined as

$$EI := \frac{1}{T_{\text{exp}}} \sum_{k=0}^{T_{\text{exp}}} \|x_k^e - x_{k,\text{ref}}^e\|_{Q_{\text{exp}}}^2 + \|u_k^e\|_{R_{\text{exp}}}^2 + (p_{y,k}^o - p_{y,k}^e),$$

where Q_{exp} and R_{exp} are cost function matrices used by all five MPC running cost $\ell(\cdot)$, whose values can be found in Table 3, and the term $(p_{y,k}^o - p_{y,k}^e)$ incurs a penalizing cost when the ego has not overtaken the opponent, and produces a reward otherwise. This index captures the time-average planning efficiency measured by a combination of tracking accuracy, control magnitude, and overtaking progress.

8.1.3 Opponent’s Policy. The opponent uses an MPC policy equipped with the shielding-aware constraint (18) to track the reference lane while avoiding colliding with the ego vehicle. The soft constraint cost weights of constraint (18) are randomized across different trials to diversify the opponent’s commitment to safety. When the ego vehicle is within a detection circle of radius r_{detect}^o , the opponent yields to the ego by changing to the other lane with a fixed probability after a time delay. Both the yielding probability and time delay are randomized across different trials. Note that the interactive behaviors produced by the opponent’s (randomized) shielding-aware MPC policy are different from, and do not use any quantity computed in the motion prediction model defined in Example 1 and used in the ST-SMPC formulation (20). Therefore, our experiments are not self-fulfilling.

8.2 Experiment Results

We start by presenting one set of representative trials (one for each planner) in Figure 14. For a fair comparison, we chose the same opponent’s policy parameters across all five trials. The ego vehicle’s reference lane is set to the inner lane for all trials. With both active uncertainty reduction and shielding-aware robust planning equipped, our proposed IDSMPC-SHARP planner produced a safe and efficient trajectory, whose quality is comparable to the one given by the Oracle MPC policy. By contrast, due to lack of shielding awareness, IDSMPC (Ablation I) produced an unsmooth and wobbling trajectory caused by triggering an emergency shielding maneuver when the ego vehicle made a hard left turn to avoid the opponent at close proximity. Since the belief state dynamics (measurement update) is removed from NDSMPC-SHARP (Ablation II), it only passively learns

the values of opponent's hidden states. As a result, the ego vehicle became overly conservative and was not able to overtake the opponent. CEMPC-SHARP (Baseline) makes decisions only based on the MAP estimate of hidden states, which is oftentimes lagging behind the opponent's actual motion. Indeed, the ego vehicle made a right turn to try to overtake the opponent from the outer lane when the MAP estimated hidden state was NY (not yielding), but the opponent showed a clear intention to make way for the ego. The right turn was therefore unnecessary and deemed inefficient for the overall planning performance.

Next, we performed a performance-safety trade-off study using the hardware experiments, and the results are plotted in Figure 13. Here, we ran 5 trials for each planner, each with a different random seed, which affects the initial conditions and opponent's policy parameters. *All trials were safe according to safety regulations SR1 and SR2.* Note that in order to account for model mismatch and communication delays, we designed a more conservative HJ Reachability shielding mechanism than SR1 and SR2, resulting in safety index $SI > 0$ for almost all trials. We see that IDSMPC-SHARP maintained a good balance between safety and efficiency, similar to that of the Oracle MPC. It is worth noticing that even the most conservative NDSMPC-SHARP policy can lead to poor safety performance. This is because, without active uncertainty reduction, SHARP was not able to effectively predict future shielding events given belief states with high uncertainty, and ultimately led the system to enter a near-unsafe region, incurring a large safety index SI . CEMPC-SHARP, due to strategy alignment, is sensitive (less robust) to belief fluctuations caused by randomness of the experiments. Therefore, its data points have the highest variance among all five planners.

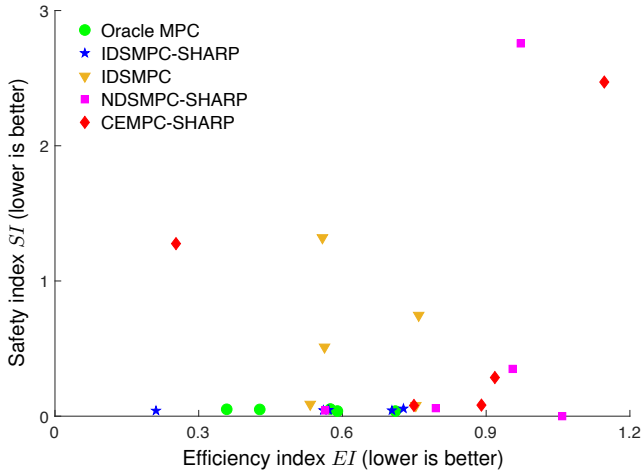


Figure 13. Performance and safety trade-off of hardware experiments (Example 1). Each data point is obtained based on the closed-loop trajectory of one trial. The lower left corner is the desired region, where both EI and SI are low.

9 Conclusions

We have introduced an implicit dual control approach towards active uncertainty reduction for interaction planning. The resulting policy improves planning efficiency via a tractable approximation to the Bellman recursion of a dual

control problem, leading to an implicit dual scenario-based SMPC policy, which automatically achieves an efficient balance between optimizing expected performance and eliciting information on future opponent's behavior.

Robust safety guarantee is obtained by wrapping the dual control policy with shielding, a supervisory safety filter. The SMPC problem is augmented with a convex shielding-aware constraint derived based on an improved variant of the recently proposed SHARP framework. The resulting IDSMPC-SHARP policy allows the ego robotic agent to efficiently interact with the opponent, while being aware of the risk of applying the costly shielding maneuvers triggered by unlikely opponent's actions. We demonstrate the proposed framework with simulated driving examples and ROS-based hardware experiments using 1/10 scale autonomous vehicles.

9.1 Limitations

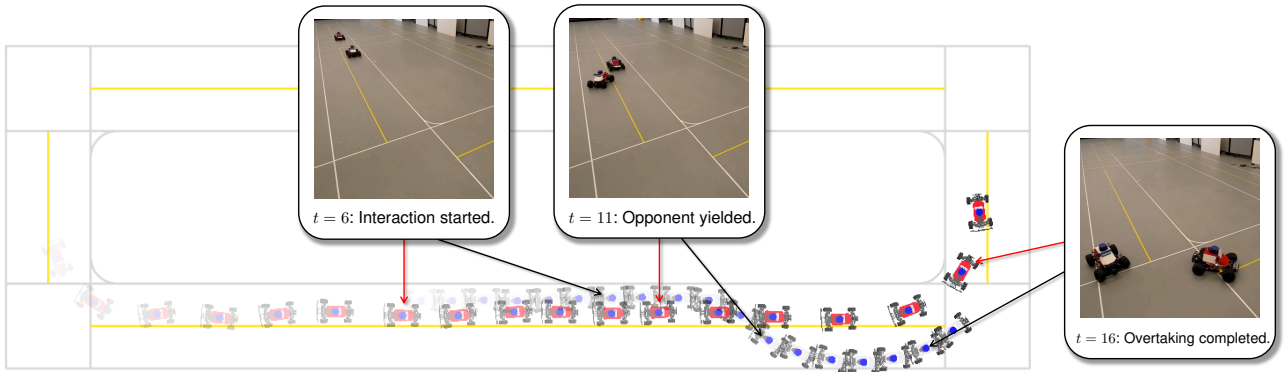
Although we have demonstrated our method on an interaction planning example with three opponents, generalizing to more agents remains an open challenge. In the worst case, the number of nodes (hence decision variables) grows exponentially with the number of interacting agents, and the number of exploration (dual control) time steps. Still, the scenario-based MPC approach is suitable for moderate-sized interaction planning problems. In addition, the current framework assumes that the ego agent can perfectly observe opponent's state and past actions, which is often unrealistic. Recent advances in interaction planning with observation uncertainties [Isele et al. \(2018b\)](#); [Sunberg and Kochenderfer \(2022\)](#) provide a promising roadmap towards improving and generalizing our method in such settings.

9.2 Future Directions

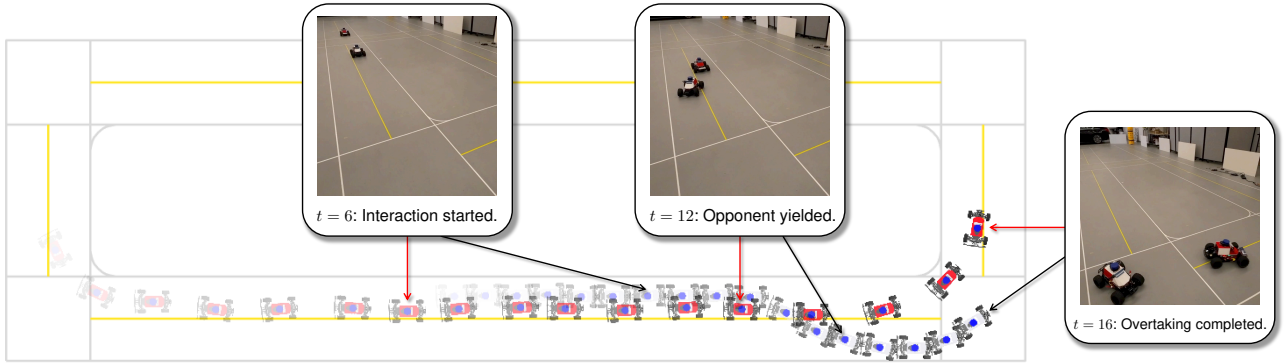
We see our work as an important step towards a broader class of methods that can handle different parametrizations of opponent's behavior from the Boltzmann rationality model, including the quantal level- k model [Stahl II and Wilson \(1994\)](#); [Tian et al. \(2021\)](#), learning-based prediction [Isele et al. \(2018a\)](#), nonlinear opinion dynamics [Bizyaeva et al. \(2022\)](#), and state- and input-dependent belief state transition dynamics $g^t(b^-, x, u^e)$ that captures the effect of ego's decisions on the opponent's hidden state. While this paper focuses on the robot's own performance, our approach may be adapted to account for social coordination and altruism [Toghi et al. \(2022\)](#) in cooperative human-robot settings. We are also excited to test our framework on other interaction planning tasks such as human-drone interaction [Fisac et al. \(2018b\)](#) with real human participants.

Acknowledgements

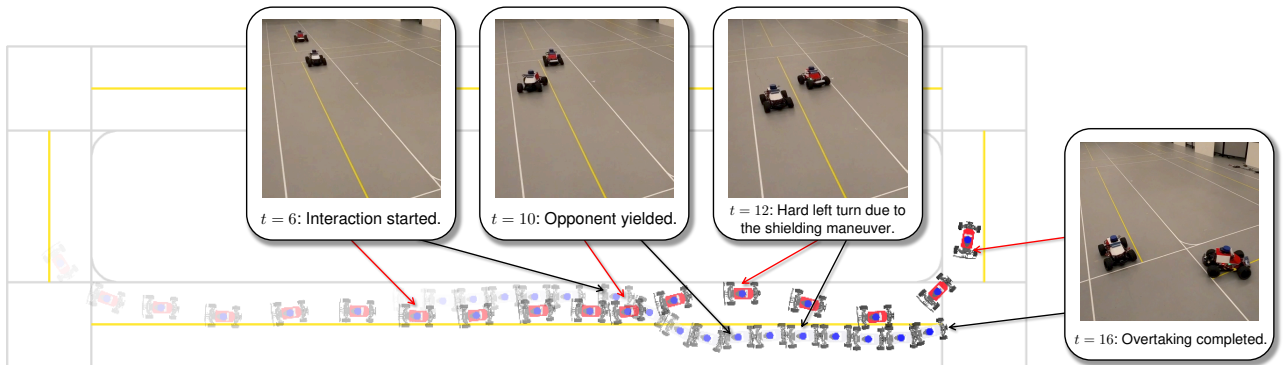
This work is supported by the Princeton SEAS Project X Innovation Fund and the Honda Research Institute (HRI) USA, Inc. This article solely reflects the opinions and conclusions of its authors and not HRI, or any other Honda entity. The authors thank Thang Lian, Huan D. Nguyen, and Zhaobo K. Zheng for their help with the hardware experiments. The authors also thank Faizan M. Tariq, Piyush Gupta, Aolin Xu, Yichen Song, Zixu Zhang, and Kai-Chieh Hsu for very helpful discussions on decision making under uncertainty, MPC, and shielding.



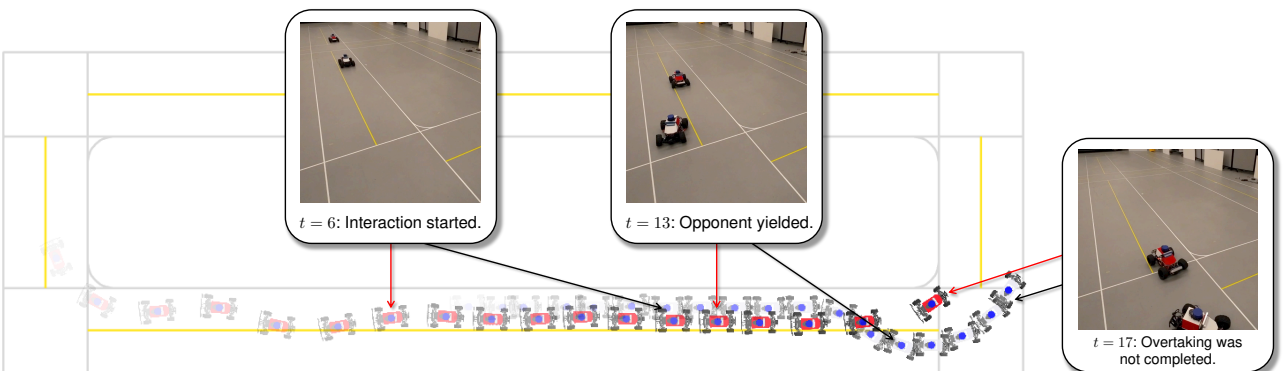
(a) Hardware experiment trial of Example 1 using Oracle MPC. Plotted trajectories are subject to minor LiDAR localization error.



(b) Hardware experiment trial of Example 1 using IDSMPC-SHARP (proposed). Plotted trajectories are subject to minor LiDAR localization error.

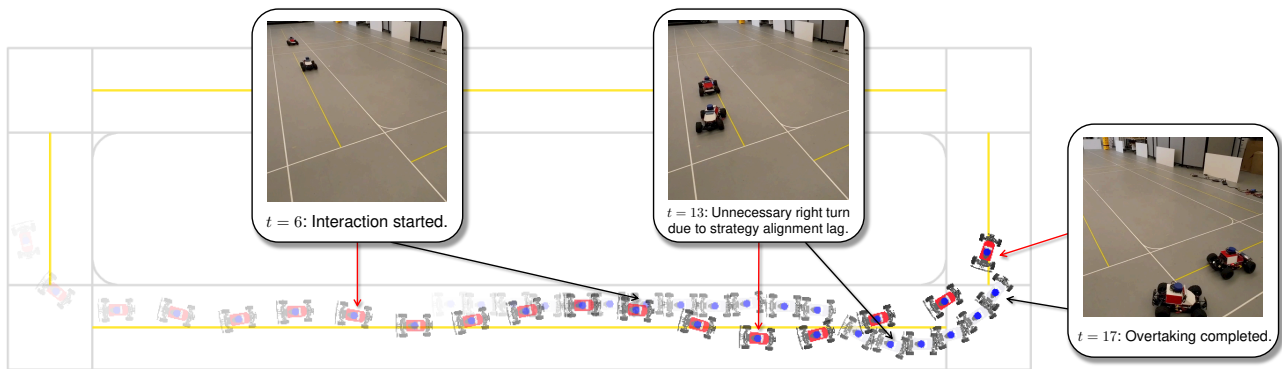


(c) Hardware experiment trial of Example 1 using IDSMPC. Plotted trajectories are subject to minor LiDAR localization error.



(d) Hardware experiment trial of Example 1 using NDSMPC-SHARP. Plotted trajectories are subject to minor LiDAR localization error.

Figure 14. Comparison between the proposed IDSMPC-SHARP planner and four other planning strategies. The ego and opponent vehicles are painted with a red and white front, respectively. Vehicle snapshots are plotted every 1 second. The proposed IDSMPC-SHARP planner accurately predicted the opponent's willingness to yield and performed a clean overtaking maneuver, comparable to the motion produced by the Oracle MPC, which computes the policy based on the opponent's communicated future plans. The IDSMPC planner (without shielding awareness) suffered performance loss due to an unforeseen emergency shielding maneuver. Without active uncertainty reduction, NDSMPC-SHARP produced an overly conservative motion and was unable to complete the overtaking task. CEMPC-SHARP is sensitive to errors in the MAP estimate of the opponent's hidden states and resulted in an unnecessary lane changing maneuver due to a lag in identifying the opponent's willingness to yield. Video can be found at <https://youtu.be/0-STmS0338c>.



(e) Hardware experiment trial of Example 1 using CEMPC-SHARP. Plotted trajectories are subject to minor LiDAR localization error.

Figure 14. Comparison between the proposed IDSMPC-SHARP planner and four other planning strategies (cont'd).

References

- Agrawal A and Sreenath K (2017) Discrete control barrier functions for safety-critical control of discrete systems with application to bipedal robot navigation. In: *Proceedings of Robotics: Science and Systems*, volume 13. Cambridge, MA, USA. DOI: 10.15607/RSS.2017.XIII.073.
- Ames AD, Xu X, Grizzle JW and Tabuada P (2016) Control barrier function based quadratic programs for safety critical systems. *IEEE Transactions on Automatic Control* 62(8): 3861–3876.
- Andersson JA, Gillis J, Horn G, Rawlings JB and Diehl M (2019) Casadi: a software framework for nonlinear optimization and optimal control. *Mathematical Programming Computation* 11(1): 1–36.
- Arcari E, Hewing L, Schlichting M and Zeilinger M (2020a) Dual stochastic MPC for systems with parametric and structural uncertainty. In: *Learning for Dynamics and Control*. pp. 894–903.
- Arcari E, Hewing L and Zeilinger MN (2020b) An approximate dynamic programming approach for dual stochastic model predictive control. *IFAC-PapersOnLine* 53(2): 8105–8111.
- Bae S, Saxena D, Nakhaei A, Choi C, Fujimura K and Moura S (2020) Cooperation-aware lane change maneuver in dense traffic based on model predictive control with recurrent neural network. In: *2020 American Control Conference (ACC)*. IEEE, pp. 1209–1216.
- Bajcsy A, Siththaranjan A, Tomlin CJ and Dragan AD (2021) Analyzing human models that adapt online. In: *2021 IEEE International Conference on Robotics and Automation (ICRA)*. IEEE, pp. 2754–2760.
- Bandyopadhyay T, Won KS, Frazzoli E, Hsu D, Lee WS and Rus D (2013) Intention-aware motion planning. In: *Algorithmic Foundations of Robotics X*. Springer, pp. 475–491.
- Bansal S, Chen M, Herbert S and Tomlin CJ (2017) Hamilton-jacobi reachability: A brief overview and recent advances. In: *IEEE Conference on Decision and Control (CDC)*. pp. 2242–2253.
- Bar-Shalom Y and Tse E (1974) Dual effect, certainty equivalence, and separation in stochastic control. *IEEE Trans. Autom. Control* 19(5): 494–500.
- Başar T and Olsder GJ (1998) *Dynamic noncooperative game theory*. SIAM.
- Baseggio M, Beghi A, Bruschetta M, Maran F and Minen D (2011) An MPC approach to the design of motion cueing algorithms for driving simulators. In: *2011 14th international IEEE conference on intelligent transportation systems (ITSC)*. IEEE, pp. 692–697.
- Bastani O (2021) Safe reinforcement learning with nonlinear dynamics via model predictive shielding. In: *2021 American Control Conference (ACC)*. IEEE, pp. 3488–3494.
- Bastani O, Li S and Xu A (2021) Safe reinforcement learning via statistical model predictive shielding. In: *Robotics: Science and Systems*.
- Bellman R (1966) Dynamic programming. *Science* 153(3731): 34–37.
- Bernardini D and Bemporad A (2011) Stabilizing model predictive control of stochastic constrained linear systems. *IEEE Trans. Autom. Control* 57(6): 1468–1480.
- Bishop CM (2006) *Pattern Recognition and Machine Learning*. Springer.
- Bizyaeva A, Franci A and Leonard NE (2022) Nonlinear opinion dynamics with tunable sensitivity. *IEEE Transactions on Automatic Control*.
- Blanchini F (1999) Set invariance in control. *Automatica* 35(11): 1747–1767.
- Bobu A, Bajcsy A, Fisac JF, Deglurkar S and Dragan AD (2020) Quantifying hypothesis space misspecification in learning from human–robot demonstrations and physical corrections. *IEEE Transactions on Robotics* 36(3): 835–854.
- Bonzanini AD, Paulson JA and Mesbah A (2020) Safe learning-based model predictive control under state- and input-dependent uncertainty using scenario trees. In: *IEEE Conference on Decision and Control (CDC)*. pp. 2448–2454.
- Bui M, Giovanis G, Chen M and Shriraman A (2022) Optimizeddp: An efficient, user-friendly library for optimal control and dynamic programming. *arXiv preprint arXiv:2204.05520*.
- Chen Y, Rosolia U, Ubellacker W, Csomay-Shanklin N and Ames AD (2022) Interactive multi-modal motion planning with branch model predictive control. *IEEE Robotics and Automation Letters* 7(2): 5365–5372.
- Chow Y, Nachum O, Duenez-Guzman E and Ghavamzadeh M (2018) A lyapunov-based approach to safe reinforcement learning. In: *Advances in Neural Information Processing Systems*. URL <https://dl.acm.org/doi/10.5555/3327757.3327904>.
- Chung SJ, Paranjape AA, Dames P, Shen S and Kumar V (2018) A survey on aerial swarm robotics. *IEEE Transactions on Robotics* 34(4): 837–855.

- Duff IS (2004) Ma57—a code for the solution of sparse symmetric definite and indefinite systems. *ACM Transactions on Mathematical Software (TOMS)* 30(2): 118–144.
- Feldbaum AA (1960) Dual control theory. i. *Avtomatika i Telemekhanika* : 1240–1249.
- Fisac JF, Akametalu AK, Zeilinger MN, Kaynama S, Gillula J and Tomlin CJ (2018a) A general safety framework for learning-based control in uncertain robotic systems. *IEEE Transactions on Automatic Control* 64(7): 2737–2752.
- Fisac JF, Bajcsy A, Herbert SL, Fridovich-Keil D, Wang S, Tomlin CJ and Dragan AD (2018b) Probabilistically safe robot planning with confidence-based human predictions. In: *Robotics: Science and Systems*.
- Fisac JF, Bronstein E, Stefansson E, Sadigh D, Sastry SS and Dragan AD (2019) Hierarchical game-theoretic planning for autonomous vehicles. In: *IEEE International Conference on Robotics and Automation (ICRA)*. pp. 9590–9596.
- Fridovich-Keil D, Ratner E, Peters L, Dragan AD and Tomlin CJ (2020) Efficient iterative linear-quadratic approximations for nonlinear multi-player general-sum differential games. In: *IEEE Int. Conf. Robot. Autom. (ICRA)*. pp. 1475–1481.
- Gill PE, Murray W and Saunders MA (2005) SNOPT: An SQP algorithm for large-scale constrained optimization. *SIAM Review* 47(1): 99–131.
- Guo H, Ji Y, Qu T and Chen H (2013) Understanding and modeling the human driver behavior based on MPC. *IFAC Proceedings Volumes* 46(21): 133–138.
- Hardy J and Campbell M (2013) Contingency planning over probabilistic obstacle predictions for autonomous road vehicles. *IEEE Transactions on Robotics* 29(4): 913–929.
- Heirung TAN, Foss B and Ydstie BE (2015) MPC-based dual control with online experiment design. *Journal of Process Control* 32: 64–76.
- Hijab O (1984) Entropy and dual control. In: *IEEE Conf. Decis. Control (CDC)*. pp. 45–50.
- Hu H and Fisac JF (2022) Active uncertainty reduction for human-robot interaction: An implicit dual control approach. In: *Algorithmic Foundations of Robotics XV*. Springer.
- Hu H, Nakamura K and Fisac JF (2022) SHARP: Shielding-aware robust planning for safe and efficient human-robot interaction. *IEEE Robotics and Automation Letters* 7(2).
- Isele D (2019) Interactive decision making for autonomous vehicles in dense traffic. In: *2019 IEEE Intelligent Transportation Systems Conference (ITSC)*. IEEE, pp. 3981–3986.
- Isele D, Nakhaei A and Fujimura K (2018a) Safe reinforcement learning on autonomous vehicles. In: *2018 IEEE/RSJ International Conference on Intelligent Robots and Systems (IROS)*. IEEE, pp. 1–6.
- Isele D, Rahimi R, Cosgun A, Subramanian K and Fujimura K (2018b) Navigating occluded intersections with autonomous vehicles using deep reinforcement learning. In: *2018 IEEE International Conference on Robotics and Automation (ICRA)*. IEEE, pp. 2034–2039.
- Kabzan J, Hewing L, Liniger A and Zeilinger MN (2019) Learning-based model predictive control for autonomous racing. *IEEE Robotics and Automation Letters* 4(4): 3363–3370.
- Klenske ED and Hennig P (2016) Dual control for approximate bayesian reinforcement learning. *The Journal of Machine Learning Research* 17(1): 4354–4383.
- Koopman P (2018) The heavy tail safety ceiling. In: *Automated and Connected Vehicle Systems Testing Symposium*, volume 1145. URL https://users.ece.cmu.edu/~koopman/pubs/koopman18_heavy_tail_ceiling.pdf.
- Lee CW, Nayer N, Garcia DE, Agrawal A and Liu B (2020) Identifying the operational design domain for an automated driving system through assessed risk. In: *2020 IEEE Intelligent Vehicles Symposium (IV)*. IEEE, pp. 1317–1322.
- Leonard NE, Paley DA, Lekien F, Sepulchre R, Fratantoni DM and Davis RE (2007) Collective motion, sensor networks, and ocean sampling. *Proceedings of the IEEE* 95(1): 48–74.
- Leung K, Schmerling E, Zhang M, Chen M, Talbot J, Gerdes JC and Pavone M (2020) On infusing reachability-based safety assurance within planning frameworks for human–robot vehicle interactions. *The International Journal of Robotics Research* 39(10-11): 1326–1345.
- Li S and Bastani O (2020) Robust model predictive shielding for safe reinforcement learning with stochastic dynamics. In: *IEEE International Conference on Robotics and Automation (ICRA)*. pp. 7166–7172. DOI:10.1109/ICRA40945.2020.9196867.
- Liniger A, Domahidi A and Morari M (2015) Optimization-based autonomous racing of 1: 43 scale rc cars. *Optimal Control Applications and Methods* 36(5): 628–647.
- Löfberg J (2004) YALMIP : A toolbox for modeling and optimization in MATLAB. In: *Proc. of the CACSD Conference*. Taipei, Taiwan.
- Luce RD (1959) *Individual Choice Behavior*. Oxford, England: John Wiley.
- Lucia S, Finkler T and Engell S (2013) Multi-stage nonlinear model predictive control applied to a semi-batch polymerization reactor under uncertainty. *Journal of process control* 23(9): 1306–1319.
- Mesbah A (2018) Stochastic model predictive control with active uncertainty learning: A survey on dual control. *Annual Reviews in Control* 45: 107–117.
- Mitchell IM, Bayen AM and Tomlin CJ (2005) A time-dependent hamilton-jacobi formulation of reachable sets for continuous dynamic games. *IEEE Transactions on automatic control* 50(7): 947–957.
- Nair SH, Govindarajan V, Lin T, Meissen C, Tseng HE and Borrelli F (2021) Stochastic MPC with Multi-modal Predictions for Traffic Intersections. *arXiv preprint arXiv:2109.09792*.
- Ong SC, Png SW, Hsu D and Lee WS (2009) Pomdps for robotic tasks with mixed observability. In: *Robotics: Science and systems*, volume 5. p. 4.
- Peters L, Fridovich-Keil D, Tomlin CJ and Sunberg ZN (2020) Inference-based strategy alignment for general-sum differential games. In: *19th International Conference on Autonomous Agents and Multi Agent Systems*. pp. 1037–1045.
- Robey A et al. (2020) Learning control barrier functions from expert demonstrations. In: *IEEE Conference on Decision and Control (CDC)*. pp. 3717–3724.
- Rubenstein M, Cornejo A and Nagpal R (2014) Programmable self-assembly in a thousand-robot swarm. *Science* 345(6198): 795–799.
- Sadigh D, Landolfi N, Sastry SS, Seshia SA and Dragan AD (2018) Planning for cars that coordinate with people: leveraging effects on human actions for planning and active information gathering over human internal state. *Autonomous Robots* 42(7): 1405–1426.

- Santos M, Diaz-Mercado Y and Egerstedt M (2018) Coverage control for multirobot teams with heterogeneous sensing capabilities. *IEEE Robotics and Automation Letters* 3(2): 919–925.
- Schildbach G and Borrelli F (2015) Scenario model predictive control for lane change assistance on highways. In: *IEEE Intelligent Vehicles Symposium (IV)*. pp. 611–616.
- Schwarting W, Pierson A, Karaman S and Rus D (2021) Stochastic dynamic games in belief space. *IEEE Transactions on Robotics* 37(6): 2157–2172.
- Sehr MA and Bitmead RR (2017) Tractable dual optimal stochastic model predictive control: An example in healthcare. In: *IEEE Conference on Control Technology and Applications (CCTA)*. pp. 1223–1228.
- Silver D and Veness J (2010) Monte-Carlo planning in large POMDPs. In: *Neural Information Processing Systems*.
- Srinivasa SS, Lancaster P, Michalove J, Schmittle M, Summers C, Rockett M, Smith JR, Chouhury S, Mavrogiannis C and Sadeghi F (2019) MuSHR: A low-cost, open-source robotic racecar for education and research. *CoRR* abs/1908.08031.
- Stahl II DO and Wilson PW (1994) Experimental evidence on players' models of other players. *Journal of economic behavior & organization* 25(3): 309–327.
- Sun P, Kretschmar H, Dotiwalla X, Chouard A, Patnaik V, Tsui P, Guo J, Zhou Y, Chai Y, Caine B et al. (2020) Scalability in perception for autonomous driving: Waymo open dataset. In: *Proceedings of the IEEE/CVF conference on computer vision and pattern recognition*. pp. 2446–2454.
- Sunberg ZN and Kochenderfer MJ (2018) Online algorithms for pomdps with continuous state, action, and observation spaces. In: *Twenty-Eighth International Conference on Automated Planning and Scheduling*.
- Sunberg ZN and Kochenderfer MJ (2022) Improving automated driving through pomdp planning with human internal states. *IEEE Transactions on Intelligent Transportation Systems*.
- Swain DT, Couzin ID and Leonard NE (2011) Real-time feedback-controlled robotic fish for behavioral experiments with fish schools. *Proceedings of the IEEE* 100(1): 150–163.
- Tian R, Sun L, Bajcsy A, Tomizuka M and Dragan AD (2022) Safety assurances for human-robot interaction via confidence-aware game-theoretic human models. In: *2022 International Conference on Robotics and Automation (ICRA)*. IEEE, pp. 11229–11235.
- Tian R, Sun L, Tomizuka M and Isele D (2021) Anytime game-theoretic planning with active reasoning about humans' latent states for human-centered robots. In: *IEEE International Conference on Robotics and Automation (ICRA)*. pp. 4509–4515.
- Todorov E and Li W (2005) A generalized iterative lqg method for locally-optimal feedback control of constrained nonlinear stochastic systems. In: *Proceedings of the 2005, American Control Conference, 2005*. IEEE, pp. 300–306.
- Toghi B, Valiente R, Sadigh D, Pedarsani R and Fallah YP (2021) Cooperative autonomous vehicles that sympathize with human drivers. In: *2021 IEEE/RSJ International Conference on Intelligent Robots and Systems (IROS)*. IEEE, pp. 4517–4524.
- Toghi B, Valiente R, Sadigh D, Pedarsani R and Fallah YP (2022) Social coordination and altruism in autonomous driving. *IEEE Transactions on Intelligent Transportation Systems*.
- Tokekar P, Vander Hook J, Mulla D and Isler V (2016) Sensor planning for a symbiotic uav and ugv system for precision agriculture. *IEEE Transactions on Robotics* 32(6): 1498–1511.
- Wabersich KP and Zeilinger MN (2021) A predictive safety filter for learning-based control of constrained nonlinear dynamical systems. *Automatica* 129: 109597.
- Wächter A and Biegler LT (2006) On the implementation of an interior-point filter line-search algorithm for large-scale nonlinear programming. *Mathematical programming* 106(1): 25–57.
- Wu C, Kreidieh AR, Parvate K, Vinitsky E and Bayen AM (2021) Flow: A modular learning framework for mixed autonomy traffic. *IEEE Transactions on Robotics*.
- Ye N, Somani A, Hsu D and Lee WS (2017) Despot: Online pomdp planning with regularization. *Journal of Artificial Intelligence Research* 58(1): 231–266.
- Zanardi A, Mion E, Bruschetta M, Bolognani S, Censi A and Frazzoli E (2021) Urban driving games with lexicographic preferences and socially efficient nash equilibria. *IEEE Robotics and Automation Letters* 6(3): 4978–4985.
- Zeilinger MN, Morari M and Jones CN (2014) Soft constrained model predictive control with robust stability guarantees. *IEEE Trans. Autom. Control* : 1190–1202.
- Zhang X, Liniger A and Borrelli F (2020) Optimization-based collision avoidance. *IEEE Transactions on Control Systems Technology* 29(3): 972–983.
- Ziebart BD, Maas AL, Bagnell JA and Dey AK (2008) Maximum entropy inverse reinforcement learning. In: *AAAI*, volume 8. pp. 1433–1438.

List of Symbols

The list below summarizes important symbols in the paper.

Interaction planning

b	Belief state
g	Belief state dynamics
g^t	Belief transition dynamics
\tilde{g}	Approximate belief state dynamics
u	Control input
d	External disturbance input
\bar{d}	Combined disturbance in parameter-affine dynamics
f	Autonomous part of joint dynamics
e	Ego
ℓ	Ego's stage cost function
ℓ_F	Ego's terminal cost function
\mathcal{I}	Information vector
o	Opponent
Q	State-action value (Q-value) function
x	Physical state
θ	Continuous hidden state

F System matrix in parameter-affine dynamics

M Discrete hidden state (mode)

Scenario tree and MPC

n Node

n_0 Root node

\mathcal{N} Node set

\mathcal{N}^d Dual control node set

\mathcal{N}^e Exploitation node set

\mathcal{N}^s Shielding node set

\mathcal{L} Leaf node set

$p(n)$ Parent node of node n

P_n Path transition probability of node n

\bar{P}_n Transition probability of node n from its parent

N Planning horizon

N^d Dual control horizon

N^e Exploitation horizon

Shielding and SHARP

\mathcal{U} Control bound

\mathcal{D} Disturbance bound

\mathcal{F} Failure set

Ω Safe (controlled-invariant) set

Ω_n Approximate local safe set at node n

π^f Safety filter policy

π^s Shielding policy

h Robust control barrier function used in SHARP

A Parameter Values

A.1 Parameter Values used in Section 7

Table 2. Planner and simulation parameters used in Section 7.

Notation	Value	Definition
Δt	0.2 s	Sampling time
l_w	3.7 m	Lane width
Q_{sim}	$\text{diag}(1, 2, 1, 1)$	Ego's state cost matrix
R_{sim}	$\text{diag}(0.1, 1)$	Ego's control cost matrix
Σ^d	$0.1I$	Disturbance covariance
N^d	2	Dual control time steps
N^e	4	Exploitation time steps
K	2	Branching number of θ^M
γ	0.5	RCBF constraint parameter used in SHARP

A.2 Parameter Values used in Section 8

Table 3. Planner and experiment parameters used in Section 8.

Notation	Value	Definition
Δt	0.2 s	Sampling time
l_w	0.6 m	Lane width
Q_{exp}	$\text{diag}(0.5, 2, 1, 1)$	Ego's state cost matrix
R_{exp}	$\text{diag}(0.1, 0.5)$	Ego's control cost matrix
Σ^d	$0.01I_8$	Disturbance covariance
N^d	3	Dual control time steps
N^e	15	Exploitation time steps
K	2	Branching number of θ^M
γ	0.5	RCBF constraint parameter used in SHARP
r_{detect}^o	2.5 m	Radius of the opponent's detection circle
\bar{t}_d^o	2.5 s	Average opponent's reaction time delay

B Proofs

B.1 Proof of Lemma 1

Recall that the combined disturbance term \bar{d}_t in (7) is a zero-mean Gaussian random variable whose covariance is defined in (10). Conditioned on $x_t \in \mathcal{I}_t$, u_t^e , and θ^M , the state distribution of x_{t+1} (likelihood) is Gaussian-distributed, i.e. $p(x_{t+1} | u_t^e, \mathcal{I}_t; \theta^M, M) \sim \mathcal{N}(\mu_{t+1}^x, \Sigma_{t+1}^x)$ whose mean and covariance are given by

$$\begin{aligned}\mu_{t+1}^x &= F(x_t, u_t^e)\theta^M + \bar{f}(x_t, u_t^e), \\ \Sigma_{t+1}^x &= \Sigma^d + B^o \Sigma_t^{u^o}(x_t, u_t^e; \theta^M) B^{o\top} = \Sigma_t^{\bar{d}}.\end{aligned}$$

Since dynamics (7) are affine in parameter θ^M , applying the self-conjugate property of Gaussian distributions yields the expression of $\mu_{t+1}^{\theta^M}$ and $\Sigma_{t+1}^{\theta^M}$. \square

B.2 Proof of Lemma 2

Let $h(\delta x) = H_n^\top \delta x$. Without loss of generality, let $\delta x_0 = x_0 - \bar{x}_0 = 0$, which implies that $h(\delta x_0) = 0$. Plugging (16) into Condition 2 in Definition 3 gives:

$$\forall \tilde{d} \in \mathcal{D} :$$

$$H_n^\top \left[(A_n + (\gamma - 1)I) \delta x + B_n^e u^e + B_n^o u^o + \tilde{d} \right] \geq 0,$$

which is satisfied if there exists $u^e \in \mathcal{U}^e$ such that:

$$\min_{\tilde{d} \in \mathcal{D}} H_n^\top \left[(A_n + (\gamma - 1)I) \delta x + B_n^e u^e + B_n^o u^o + \tilde{d} \right] \geq 0,$$

where the optimal disturbance d^* is given by (19). Therefore, map $h(\delta x)$ is a valid discrete-time Exponential RCBF for system (16) and safe set Ω_n . Using Proposition 4 in Agrawal and Sreenath (2017) we conclude that Ω_n is robust controlled-invariant. \square

C Practical Aspects

C.1 Computing Opponent's Rational Action

The Laplace approximation used by (8) requires the mean function (human's rational action) $\mu_i^M(x_t, u_t^e)$ as the

maximizer of the basis Q-value function $Q_i^M(u_i^{M,o}; x_t, u_t^e)$. In our paper, we use the game-theoretic approach [Fridovich-Keil et al. \(2020\)](#) as the backend to compute $Q_i^M(\cdot)$ online, which adopts an analytical maximizer. In case when the expression of $\mu_i^M(\cdot)$ cannot be computed beforehand, we use a numerical approach similar to [Sadigh et al. \(2018\)](#), which computes a *local* maximizer $\mu_i^M(\cdot)$ during online optimization. Under the mild assumption that $Q_i^M(\cdot)$ is a smooth function whose maximum can be attained, we can set the gradient of $Q_i^M(\cdot)$ with respect to u_i^M to 0. This condition can be enforced either as a differential-algebraic equation (DAE) constraint [Andersson et al. \(2019\)](#) or a penalty cost in ST-SMPC problem (20).

C.2 Projecting Predicted Opponent's Action

Using the approximate opponent's action model (9) constraint $u_n^o \in \mathcal{U}^o$ in (20) may not be feasible, since the predicted human's action u_n^o is given as a weighted sum of (unbounded) basis functions with (unbounded) normally distributed weights. To reconcile this, we define, for each node \tilde{n} , two separate decision variables: \tilde{u}_n^o , which must equal the sampled linear combination of basis functions, and u_n^o , which must satisfy $u_n^o \in \mathcal{U}^o$. By adding a cost term $C\|\tilde{u}_n^o - u_n^o\|_2$ to (20), with some large $C > 0$ (we use $C = 10^8$), the solver sets u_n^o to the nearest point in \mathcal{U}^o to the sample-consistent \tilde{u}_n^o . This feasible “projected” control u_n^o enters the dynamics in (20).

C.3 Initialization Pipeline

Since problem (20) is in general a large-scale nonconvex optimization problem, initialization is crucial for solving it rapidly and reliably in real time. In this paper, we generate an initial guess for (20) using the following pipeline:

1. (Optional) Solve a certainty-equivalent MPC by setting θ^M and M to their maximum a posteriori estimated values based on the current belief state \hat{b}_t .
2. Solve a non-dual SMPC with the same scenario tree structure as the dual-SMPC, replacing belief state dynamics $\tilde{g}(\cdot)$ with $g^t(\cdot)$ for all dual control steps, and using the certainty-equivalent MPC solution as the initial guess.
3. Forward-propagate belief states through $\tilde{g}(\cdot)$ using the non-dual SMPC solution for all dual control nodes in the scenario tree.

Step 1 is optional and is only needed when the non-dual SMPC in Step 2 cannot be readily solved. In Section 7 and 8, we show that even if (20) uses results of the non-dual SMPC as its initialization, the resulting closed-loop trajectories are significantly different.